International Journal of Applied Engineering
Research and Development (IJAERD)
ISSN(P): 2250-1584; ISSN(E): 2278-9383
Vol. 7, Issue 1, Feb 2017, 1-36

TRANS STELLAR
•Journal Publications •Research Consultancy

Original Article

STUDY ON DYNAMIC STABILITY AND FREE VIBRATIONS OF MULTI-SPAN FLUID-CONVEYING PIPES IN WATER WITH VARIOUS END CONDITIONS

JONG-SHYONG WU[1], JEE-RAY WANG[2], DER-WEI CHEN[3] & CHING-AN HUANG[4]

[1,4]*Department of Systems and Naval Mechatronic Engineering,*
National Cheng-Kung University, Tainan, Taiwan
[2]*Department of Automation Engineering and Institute of Mechatronoptic,*
Chienkuo Technology University, Changhua, Taiwan
[3]*Department of Power Vehicle and Systems Engineering, Chung-Cheng Institute of Technology,*
National Defense University, Dashi, Taoyuan, Taiwan

ABSTRACT

The literature regarding transverse vibrations of fluid-conveying pipes in air is plenty, however, most of them is for the stability of single-span clamped-free (C-F) pipes, and the reports relating to the critical flow velocities of the multi-span fluid-conveying pipes (either in air or in water) with various end supports are not found yet, thus, this paper tries to study the title problem by using the finite element method (FEM). First of all, the property matrices of an axial-loaded fluid-conveying pipe element in water are derived through application of the Lagrange's equation. Next, the assembly technique is used to construct the overall mass, damping and stiffness matrices for the entire fluid-conveying pipe, and after imposing the total constrained degrees of freedom (DOFs), the equations of motion for the entire multi-span fluid-conveying pipe are obtained. Solution of the latter equations of motion will produce the complex eigenvalues and complex eigenvectors, with the imaginary part of each eigenvalue and the real part of each eigenvector denoting the damped natural frequency and damped mode shape, respectively. To confirm the reliability of the presented approach, the stability curve, the Argand diagrams for several complex eigenvalues and the associated dimensionless critical flow velocities of a single-span pipe with three (end) boundary conditions (BCs) are determined and compared with the existing literature, and good agreement is achieved. For a "q-span" pipe ($q = 1,2,3,...$) with equal span lengths and S end supports (or BCs), it has been found that, its first dimensionless critical flow velocity $^{(q)}_{S}U^{*}_{1,cr}$ leading to buckling can easily be determined from the Argand diagram associated its 1st complex eigenvalue λ_1, and this is not true for a classical axial-loaded "q-span" beam on the basis of static-stability theory. Furthermore, for the last pipe with pinned-pinned (P-P) end supports, it has been found that the first dimensionless critical flow velocity is given by $^{(q)}_{PP}U^{*}_{1,cr} = q\pi$. In addition to the stability analyses, the determination of damped natural frequencies and damped mode shapes of a multi-span fluid-conveying pipe (with Coriolis effect considered) in three BCs is also illustrated. Since the information regarding the dynamic behaviors of the multi-span fluid-conveying pipes (either in air or in water) is rare, the presented approach and the obtained results will be useful in the practical applications.

KEYWORDS: Multi-Span Pipe, Stability, Critical Flow Velocity, Argand Diagram, Damped Natural Frequency and Mode Shape, Finite Element Method

Received: Nov 30, 2016; **Accepted:** Jan 05, 2017; **Published:** Jan 19, 2017; **Paper Id.:** IJAERDFEB20171

1. INTRODUCTION

The dynamic behaviors of the fluid-conveying pipes are the important information for the engineers, thus, the reports concerned are numerous. In the work of Ibrahim [1], more than four hundred reports regarding various fluid-conveying pipes are reviewed and it is found that most of them are for the *single-span* pipes with cantilevered conditions as one may see from the list of references. In early years, Chen [2], Paidoussis and Issid [3], Ting and Hosseinipour [4], Paidoussis et al. [5], Chen and Fan [6], Pramila et al. [7], Dupuis and Rousselet [8], To and Healy [9], Pramila [10], Chang and Cheng [11], and Bratt [12] will be some of the pioneers for the dynamic analyses of *single-span* pipes and only a few reports regarding the *multi-span* pipes, such as the works of Stein and Tobriner [13], Singh and Mallik [14,15], Koo and Park [16], Wu and Shih [17] and Wu et al. [18]. From the existing literature one sees that the dynamic behaviors of most *single-span* pipes are studied by using the assumed mode (or modal analysis) method [2-4,18] or the FEM [6-10,18], but those of the periodically supported multi-span pipes are investigated with the wave approach [14-16], in which, the dynamic equation for any span of a periodically supported multi-span pipe is assumed to be the same so that the CPU time of computations is independent on the total number of spans, however, this assumption may disagree with the realistic conditions. In the work of Wu and Shih [17], the transfer matrix method (TMM) [19], the mode superposition method [20] and the Newmark direct integration method [21] are used to determine the natural frequencies and mode shapes of the undamped multi-span pipe as well as the forced vibration responses of the damped one with Coriolis force considered. Although the formulation of [17] is more practical, but the stability analysis of the multi-span fluid-conveying pipe is not performed. Thus, in Ref. [18], Wu et al. have studied the last problem, but only the 3-span pipe in air and with pinned-pinned (P-P) end conditions was studied.

From the foregoing literature review, it is seen that the reports relating to the *critical* flow velocities of the *multi-span* fluid-conveying pipes (either in air or in water) with "various" end supports (or BCs) do not appear yet, thus, this paper tries to present some information in this aspect. First of all, the property matrices of an *axial-loaded* fluid-conveying pipe element in water are derived through application of the Lagrange's equation [22-26]. Here, for simplicity, the main effect of the surrounding water on the fluid-conveying pipe is assumed to be distributed on the *added mass* [27,28]. Next, the assembly technique is used to construct the overall mass, damping and stiffness matrices for the entire fluid-conveying pipe, and after eliminating all constrained degrees of freedom (DOFs), the equations of motion for the entire pipe system to take the form $[\overline{m}]\{\ddot{\overline{u}}\}+[\overline{c}]\{\dot{\overline{u}}\}+[\overline{k}]\{\overline{u}\}=0$ is obtained. For convenience, the last equations are transformed into another form $[M]\{\dot{\overline{Y}}\}+[K]\{\overline{Y}\}=0$ [22] and then the existing approach is used to solve the eigenproblem [29]. Because of the effects of Coriolis force and the inner (or outer) damping, the eigenvalues and eigenvectors of the last equations are the complex numbers. Numerical examples reveal that the *imaginary* part of each complex eigenvalue denotes the *damped* natural frequency and the *real* part of each corresponding complex eigenvector denotes the associated *damped* mode shape. In the stability analysis, it is found that, for a "*q*-span" fluid-conveying *pipe* ($q=1,2,3,...$) with *S* end supports (S = P-P, C-C (clamped-clamped) or C-P (clamped-pinned)), if its "*k*th" buckled mode shape ${}^{(q)}_{S}\hat{Y}_k(x)$ takes the same form as the "*r*th" buckled mode shape ${}_{S}\hat{Z}_r(x)$ of a *classical* axial-loaded "1-span" *beam* with the same *S* end supports obtained from the theory of *static* stability [30], i.e., ${}^{(q)}_{S}\hat{Y}_k(x)={}_{S}\hat{Z}_r(x)$, then the *k*th *critical* "dimensionless" flow velocity ${}^{(q)}_{S}U^*_k$ of the "*q*-span" fluid-conveying *pipe* is equal to the "*r*th" *equivalent* one ${}_{S}V^*_r$ of the classical axial-loaded "1-span" *beam*, i.e.,

${}_S^{(q)}U_k^* = {}_SV_r^*$. For convenience, the *statically* applied axial load $N = m_f V^2$ associated with the *r*th critical dimensionless flow velocity ${}_SV_r^*$ of the classical axial-loaded "1-span" *beam* is called the "equivalent" axial load and derived in the ***Appendix*** at the end of this paper, where m_f denotes the fluid mass (inside the pipe) per unit length and $V = U$ denotes the "dimensional" flow velocity. In addition to the stability analysis, the free vibration characteristics of a 4-span fluid-conveying pipe with three kinds of end supports (or BCs) are also investigated.

To confirm the presented approach and the developed computer programs for this paper, the stability curve, the Argand diagrams of several complex eigenvalues and the associated critical "dimensionless" flow velocities of instability (or buckling) for an "1-span" fluid-conveying pipe with pinned-pinned (P-P), clamped-clamped (C-C) and clamped-free (C-F) end supports are determined and compared with the available literature, and good agreement is achieved. It is noted that, the *mode shapes* corresponding to the "damped" natural frequencies of either single-span or multi-span fluid-conveying pipe (with Coriolis effect considered) are not presented in most of the existing literature, however, they do appear in this paper.

2. FORMULATION OF THE PROBLEM

This section includes the assumptions, the derivation of property matrices of the *axially loaded* pipe element in water, the constrained DOFs for various supporting conditions and the equations of motion for the entire multi-span fluid-conveying pipe along with their solutions.

2.1 Assumptions for the Formulation

The formulation of this paper is based on the following assumptions [2,3]: (a) The pipe is made of homogeneous Kelvin-Voigt viscoelastic material; (b) The fluid is incompressible and inviscid; (c) The effect of the pipe motion on the fluid is negligible; (d) The velocity profile of the fluid is uniform over the cross-sectional area of the pipe (i.e., the plug-flow type). In addition to the last assumptions for the fluid-conveying pipes in air, for simplicity, we also assumed that the main effect of the surrounding water on a fluid-conveying pipe is distributed on the *added mass* [27,28].

2.2 Property Matrices of an Axial-Loaded Pipe Element

Figure 1(a) shows the mathematical model of a *q*-span uniform fluid-conveying pipe submersed in water with P-P supports in the global coordinate system $\overline{xy}$, in which, the symbols 1, 2, …, S_{i-1}, …, S_i, …, S_{i+1}, …, *n* and *n*+1 dente the numberings of *nodes*, and (1), (2), …, (*i*), (i+1), …, (*q-1*) and (*q*) denote those of *spans*. Figure 1(b) shows a typical two-node 4-DOF pipe element subjected to the axial load *N* in the local coordinate system xy, in which, $u_y = u_y(x,t)$ denotes the element displacement at position x and time *t*, u_j (j = 1 to 4) denote the nodal displacements, and ℓ denotes the element length. According to the assumptions given in the last subsection, the kinetic energy *T* and potential energy *V* of the fluid-conveying pipe element shown in Figure 1(b) are given by [7,24,26]:

$$T = \tfrac{1}{2}\int_0^{\ell}(m_p + m_a + m_f)\dot{u}_y^2 dx + \int_0^{\ell} m_f U \dot{u}_y u_y' dx + \tfrac{1}{2}\int_0^{\ell} m_f U^2 u_y'^2 dx \tag{1}$$

$$V = \tfrac{1}{2}\int_0^{\ell} EI u_y''^2 dx - \tfrac{1}{2}\int_0^{\ell}(P_p + p_f A_f) u_y'^2 dx \tag{2}$$

Furthermore, the non-conservative virtual work done by the damping forces is given by [2,3]

$$\delta W_{nc} = -\int_0^{\ell} \hat{E} I \dot{u}_y'' \delta u_y'' dx - \int_0^{\ell} C_o \dot{u}_y \delta u_y dx \tag{3}$$

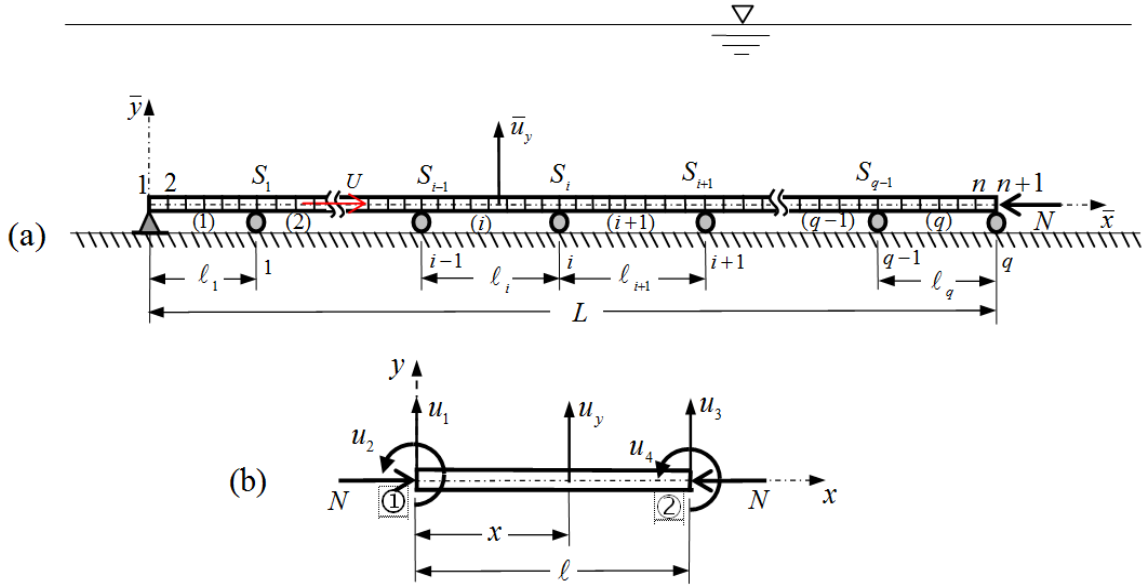

Figure 1: (a) The Mathematical Model for a *q*-Span Uniform Fluid-Conveying Pipe in Water with P-P Supports in the Global Coordinate System $\bar{x}\bar{y}$, with 1,2, …, S_{i-1},…, S_i ,…, S_{i+1},…, *n* and *n*+1 Denting the Numberings of *Nodes*, and (1), (2), …, (*i*), (i+1), …, (*q-1*) and (*q*) Denoting Those of *Spans*; (b) the Two-Node 4-DOF Pipe Element Subjected to the Axial Load *N* in the Local Coordinate System xy, with $u_y = u_y(x,t)$ Denoting the Element Displacement and u_j (j = 1 to 4) Denoting the Nodal Displacements

In Eq. (1), m_p, m_a and m_f are the *pipe* mass, *added* mass and *fluid* mass per unit length, respectively, U is the constant axially flow velocity, u_y' and $\dot{u}_y$ are the differentiations of $u_y(x,t)$ with respect to coordinate x and time t, respectively. In Eq. (2), E and I are Young's modulus and moment of inertia of cross-sectional area of the pipe wall, respectively, P_p is the externally applied axial force on the pipe wall with the *compressive* one to be positive (+), p_f is the pressure intensity of fluid (inside the pipe), and A_f is the inner cross-sectional area of pipe (or cross-sectional area for flowing fluid). Note that, in Eq. (1), the 2nd and 3rd terms are due to the Coriolis force and centrifugal force of fluid, respectively. In Eq. (3), $\hat{E}$ is the coefficient of internal dissipation of the pipe material and C_o is the coefficient of external viscous damping due to friction between the pipe and the flowing fluid.

According to Refs. [20,23], one has the following relationships

$$u_y = [a_y]\{u\} \tag{4}$$

where

$$\{u\} = \{u_1 \quad u_2 \quad u_3 \quad u_4\} = [u_1 \quad u_2 \quad u_3 \quad u_4]^T, \qquad [a_y] = [a_{u1} \quad a_{u2} \quad a_{u3} \quad a_{u4}] \tag{5a,b}$$

In Eq. (5b), $[a_y]$ is the *shape function* matrix with its coefficients given by

$$a_{u1}(\xi)=1-3\xi^2+2\xi^3,\ a_{u2}(\xi)=(\xi-2\xi^2+\xi^3)\ell,\ a_{u3}(\xi)=3\xi^2-2\xi^3,\ a_{u4}(\xi)=(-\xi^2+\xi^3)\ell \quad (6a\text{-}d)$$

with

$$\xi = x/\ell \quad (7)$$

Where x is the axial local coordinate and ℓ is the element length as shown in Figure 1(b).

From Eqs. (3) and (4), one obtains the non-conservative generalized force vector

$$\{Q_{nc}\} = -\int_0^{\ell} \widehat{E}I[a_y'']^T[a_y'']dx\cdot\{\dot{u}\} - \int_0^{\ell} C_o[a_y]^T[a_y]dx\cdot\{\dot{u}\} \quad (8)$$

Now, substituting Eq. (4) into Eqs. (1) and (2), respectively, then introducing the resulting expressions for kinetic energy T and potential energy V as well as the generalized force $\{Q_{nc}\}$ given by Eq. (8) into the next Lagrange's equation [22] with $z = z_1 = \{u\}$

$$\frac{d}{dt}\left(\frac{\partial T}{\partial \dot{z}_r}\right) - \frac{\partial T}{\partial z_r} + \frac{\partial V}{\partial z_r} = Q_{r,nc},\ r = 1,2,3,...,n \quad (9)$$

One obtains the equations of motion for the pipe element shown in Figure 1(b) to be

$$[m]_e\{\ddot{u}\}_e + ([C_c]_e^T - [C_c]_e)\{\dot{u}\}_e + [k]_e\{u\}_e = -[C_d]_e\{\dot{u}\}_e \quad (10)$$

or

$$[m]_e\{\ddot{u}\}_e + [c]_e\{\dot{u}\}_e + [k]_e\{u\}_e = 0 \quad (11)$$

Where the subscript "e" refers to the pipe "element" and

$$[m]_e = (m_p + m_a + m_f)\int_0^{\ell}[a_y]^T[a_y]dx \quad (12)$$

$$[c]_e = ([C_c]_e^T - [C_c]_e) + [C_d]_e \quad (13)$$

$$[k]_e = [k_B]_e - [k_G]_e \quad (14)$$

with

$$[C_c]_e = m_f U\int_0^{\ell}[a_y']^T[a_y]dx,\ [C_d]_e = \hat{E}I\int_0^{\ell}[a_y'']^T[a_y'']dx + C_o\int_0^{\ell}[a_y]^T[a_y]dx \quad (15a,b)$$

$$[k_B]_e = EI\int_0^{\ell}[a_y'']^T[a_y'']dx \quad ,\ [k_G]_e = N\int_0^{\ell}[a_y']^T[a_y']dx,\ N = P_p + m_f U^2 + p_f A_f \quad (16a\text{-}c)$$

In Eq. (16c), N denotes the total effective axial load due to the externally applied force P_p, the centrifugal force $m_f U^2$ and the fluid pressure $p_f A_f$. For the case of $P_p = p_f A_f = 0$, the buckling of the fluid-conveying pipe is due to the centrifugal force $m_f U^2$ and the corresponding value of U is called the *critical* flow velocity U_{cr}.

2.3 Constrained DOFs for Various BCs

For the multi-span fluid-conveying pipe composed of n elements and $n+1$ nodes as shown in Figure 1(a), its constrained DOFs associated with the BCs are as follows:

- For the pinned-pinned (P-P) pipe, one has $\bar{u}_1 = 0$ at the first node 1 and $\bar{u}_{2n+1} = 0$ at the final node $n+1$. Thus, the numberings for the constrained DOFs are: 1 and $2n+1$.
- For the clamped-clamped (C-C) pipe, one has $\bar{u}_1 = \bar{u}_2 = 0$ at the first node 1 and $\bar{u}_{2n+1} = \bar{u}_{2n+2} = 0$ at the final node $n+1$. Thus, the numberings for the constrained DOFs are: 1, 2, $2n+1$ and $2n+2$.
- For the clamped-pinned (C-P) pipe, one has $\bar{u}_1 = \bar{u}_2 = 0$ at the first node 1 and $\bar{u}_{2n+1} = 0$ at the final node $n+1$. Thus, the numberings for the constrained DOFs are: 1, 2 and $2n+1$.
- For the clamped-free (C-F) pipe, one has $\bar{u}_1 = \bar{u}_2 = 0$ at the first node 1 only. Thus, the numberings for the constrained DOFs are: 1 and 2.

In addition to the foregoing constrained DOFs associated with the end supports (or BCs) of the entire pipe, there is one DOF at each intermediate pinned support i is also constrained. If the numbering for the above pinned support i is S_i as shown in Figure 1(a), then the numbering for the corresponding constrained DOF is "$2S_i - 1$". It is evident that, for a "q-span" pipe, there are $q-1$ intermediate pinned supports and the $q-1$ DOFs corresponding these supports must also be eliminated for obtaining the *effective* property matrices of the entire pipe system, in addition to the DOFs corresponding to each specified BCs.

2.4 Equations of Motion for the Entire Pipe System and Their Solutions

Assembling all the element property matrices obtained from previous **Subsection 2.2**, one can determine the overall mass matrix [m], damping matrix [c] and stiffness matrix [k] for the entire multi-span fluid-conveying pipe, and eliminating the rows and columns associated with the constrained DOFs for the specified BCs and the intermediate pinned supports shown in the last **Subsection 2.3**, one may obtain the system equations of motion to take the form

$$[\bar{m}]\{\ddot{\bar{u}}\} + [\bar{c}]\{\dot{\bar{u}}\} + [\bar{k}]\{\bar{u}\} = 0 \tag{17}$$

where, $[\bar{m}]$, $[\bar{c}]$ and $[\bar{k}]$ are the overall *effective* mass, damping and stiffness matrices of the entire pipe system, obtained from [m], [c] and [k] by eliminating the rows and columns associated with all the constrained DOFs, respectively. For free vibrations, one has

$$\{\bar{u}\} = \{\bar{u}(t)\} = \{Y\}e^{j\omega t} \tag{18}$$

Where $\{Y\}$ is the amplitude vector of $\{\bar{u}(t)\}$, ω is the "damped" natural frequency of the entire pipe system, t is time and $j = \sqrt{-1}$. In order to use the existing approach [29] to solve Eq. (17), one requires to transform the latter into the form below [22]

$$[M]\{\dot{\bar{Y}}\} + [K]\{\bar{Y}\} = 0 \tag{19}$$

Where

$$[M]=\begin{bmatrix}[0] & [\overline{m}]\\ [\overline{m}] & [\overline{c}]\end{bmatrix},\ [\overline{K}]=\begin{bmatrix}-[\overline{m}] & [0]\\ [0] & [\overline{k}]\end{bmatrix},\ \{\overline{Y}\}=\begin{Bmatrix}\{\dot{\overline{u}}\}\\ \{\overline{u}\}\end{Bmatrix},\ \{\dot{\overline{Y}}\}=\begin{Bmatrix}\{\ddot{\overline{u}}\}\\ \{\dot{\overline{u}}\}\end{Bmatrix} \tag{20a-d}$$

With respect to each specified fluid velocity U, the *r*th eigenvalue ω_r and the associated *r*th eigenvector $\{\overline{Y}_r\}$ of Eq. (17) take the pairs of conjugate complex numbers

$$\omega_r=\omega_{r,R}\pm j\omega_{r,I},\ \{\overline{Y}_r\}=\begin{Bmatrix}\omega_{r,R}\overline{Y}_{r,R}\\ \overline{Y}_{r,R}\end{Bmatrix}\pm j\begin{Bmatrix}\omega_{r,I}\overline{Y}_{r,I}\\ \overline{Y}_{r,I}\end{Bmatrix} \tag{21a,b}$$

The *imaginary* part of ω_r, $\omega_{r,I}$, denotes the *r*th natural frequency and the corresponding *real* part of $\{\overline{Y}_r\}$, $\{\overline{Y}_{r,R}\}$, denotes the *r*th mode shape.

It is noted that, for a single-span cantilevered (C-F) pipe with $P_p+p_fA_f=0$, the following momentum transport at the downstream "free end" must be considered: $m_fU^2u_y'+m_fU\dot{u}_y|_{x=L}$ [6,24-26]. In other words, for a cantilevered pipe consisting of n elements and $n+1$ nodes (cf. Figure 1(a)), its total DOFs is $2(n+1)$ before imposing the constrained DOFs, thus, one must add $k_{2n+1,2n+2}=m_fU^2$ and $c_{2n+1,2n+1}=m_fU$ to the corresponding coefficients of the overall stiffness matrix $[k]$ and overall damping matrix $[c]$, respectively. It is evident that the effects of m_fU^2 and m_fU on the pinned or clamped BC at right end of the pipe are nil, if the (2n+1)th DOF is constrained.

The relationship between the *r*th dimensionless frequency λ_r and the corresponding dimensional one ω_r is given by

$$\lambda_r=\omega_rL^2\sqrt{m_{tot}/(EI)} \tag{22a}$$

Where

$$m_{tot}=m_p+m_a+m_f \tag{22b}$$

And for convenience, the following dimensionless parameters are introduced

$$m_f^*=\frac{m_f}{m_{tot}},\ U^*=UL\sqrt{\frac{m_f}{EI}},\ \hat{E}^*=\left(\frac{\hat{E}}{L^2}\right)\sqrt{\frac{I}{m_{tot}E}},\ C_o^*=\frac{C_oL^2}{\sqrt{m_{tot}EI}} \tag{23a,b,c,d}$$

In Eq. (22b), the symbol m_{tot} denotes the *total* mass per unit length. It is composed of three components given by

$$m_P=\tfrac{1}{4}\rho_P\pi(d_o^2-d_i^2),\ m_a=\tfrac{1}{4}C_a\rho_w\pi d_o^2,\ m_f=\tfrac{1}{4}\rho_f\pi d_i^2 \tag{24a,b,c}$$

Where ρ_P, ρ_w and ρ_f are mass densities of *pipe* (material), *water* (outside the pipe) and *fluid* (inside the pipe), respectively; d_o and d_i are the outer and inner diameters of the pipe, respectively; and C_a is the *added mass coefficient*. For the circular cross-section, one may set $C_a\approx1.0$ [27,28].

3. NUMERICAL RESULTS AND DISCUSSIONS

For simplicity, we set $\hat{E} = C_0 = 0$ in this paper, and before the stability and free vibration analyses of the multi-span fluid-conveying pipes, some numerical results are compared with the available existing literature first. The dimensions and physical properties of the pipes are: outer diameter $d_o = 0.254$ m, inner diameter $d_i = 0.2286$ m, Young's modulus $E = 2.068\times10^{11}$ N/m^2 and mass density of pipe $\rho_p = 7850$ kg/m^3 . The mass density of water is assumed to be $\rho_w = 1000$ kg/m^3 and the mass density of fluid, ρ_f , corresponding to each specified mass ratio m_f^* is determined from Eqs. (22b), (23a) and (24a,b,c). Note that the fluid-conveying pipes are in water unless it is indicated that "in air (with $\rho_w = 0$)".

3.1 Validation of Presented Method and Developed Computer Program

3.1.1 *Free Vibration of the Axial-Loaded Multi-Span Pipe Filled with Still Fluid*

For a multi-span pipe with *equal* span lengths ℓ_0 and hinged end supports in air (with $\rho_w = 0$), and filled with *still* fluid, its lowest buckling load $P_{1,cr}$ and fundamental frequency $\omega_{0,1}$ are given by [31]

$$P_{1,cr} = (\pi/\ell_0)^2 EI\ ,\ \omega_{0,1} = (\pi/\ell_0)^2\sqrt{EI/(\rho_p A_p + \rho_f A_f)} \tag{25a,b}$$

If $\rho_f = 1000$ kg/m^3 and $\ell_0 = 6$ m, then $P_{1,cr} = 3.983682\times10^6$ N and $\omega_{0,1} = 96.77358$ rad/sec. For the case of $U = 0$ and $p_f = 0$, Table 1 shows the lowest four natural frequencies of the P-P pipe with 1-, 2-, 3- and 4- span and subjected to the axial load $N = 0.6P_{1,cr} = 2.3902092\times10^6$ N, respectively, as shown in Figure 2(a)-(d). In Table 1, $\omega_{N,r}$ and $\omega_{0,r}$ denote the *r*th natural frequencies of the pipe with and without subjecting to the axial load *N*, furthermore, $\omega_{N,r}/\omega_{0,r}$ denotes the frequency ratio between $\omega_{N,r}$ and $\omega_{0,r}$ obtained from the presented FEM and [31], respectively. Among the values of $\omega_{N,r}/\omega_{0,r}$ obtained from [31], those with *four* decimal places (e.g., $\omega_{N,r}/\omega_{0,r}$ = 0.8436) are given by Tables 1-5 of [31], and those with *two* decimal places (e.g., $\omega_{N,r}/\omega_{0,r}$ = 0.6300 =0.63) are given by Figure 5-8 of [31]. From the Table 1 one sees that the frequency ratios ($\omega_{N,r}/\omega_{0,r}$) obtained from the presented FEM (with number of pipe elements "for each span" to be $n_1 = 50$) are in good agreement with the corresponding ones obtained from [31].

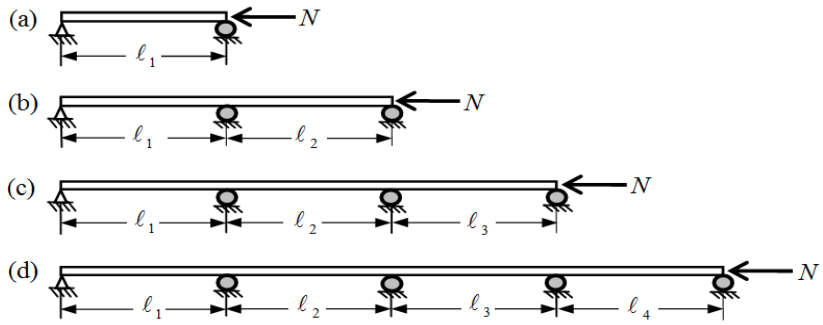

Figure 2: The Four Uniform P-P Pipes (in air) Filled with *Still* Fluid and Subjected to Axial Load N with *Equal* Span Lengths $\ell_1 = \ell_2 = \ell_3 = \ell_4 = \ell_0$: (a) 1-span with $L = \ell_0$; (b) 2-Span with $L = 2\ell_0$; (c) 3-Span with $L = 3\ell_0$; (d) 4-Span with $L = 4\ell_0$. Where *L* is the Total Length of the Entire (Multi-Span) Pipe

Table 1: Influence of Axial Load $N = 0.6P_{1,cr} = 2.3902092\times10^6$ N on the Lowest Four Natural Frequencies (rad/sec) of the Entire pipe (in Air) Filled with *Still* Fluid and with 1 to 4 Spans in the Hinged Supporting Conditions as Shown in Figs. 2(a)-(d) (with $U = 0$, $p_f = 0$, $\rho_w = 0$, $\rho_f = 1000$ kg/m^3 and $\ell_0 = 6$ m)

No. of spans q	Total length L (m)	Methods	Frequency (or ratio)	No. of pipe elements $n_e = n_1 q$	Mode No., r			
					1	2	3	4
1 Figure2(a)	6	FEM	[a] $\omega_{0,r}$	50×1	96.7736	387.0944	870.9630	1548.3817
			[b] $\omega_{N,r}$		61.2050	356.8834	841.4303	1519.0723
		FEM	$\omega_{N,r}/\omega_{0,r}$		0.6325	0.9220	0.9661	0.9811
		Ref. [31]		—	0.6300	0.9200	0.9700	—
2 Figure2(b)	6×2	FEM	$\omega_{0,r}$	50×2	96.7736	151.1788	387.0944	489.9163
			$\omega_{N,r}$		61.2050	127.5324	356.8834	464.3150
		FEM	$\omega_{N,r}/\omega_{0,r}$		0.6325	0.8436	0.9220	0.9477
		Ref. [31]		—	0.6325	0.8436	0.9220	—
3 Figure2(c)	6×3	FEM	$\omega_{0,r}$	50×3	96.7736	124.0168	181.0902	387.0944
			$\omega_{N,r}$		61.2050	96.3617	160.4495	356.8834
		FEM	$\omega_{N,r}/\omega_{0,r}$		0.6325	0.7770	0.8860	0.9220
		Ref. [31]		—	0.6325	0.7700	0.8800	—
4 Figure2(d)	6×4	FEM	$\omega_{0,r}$	50×4	96.7736	112.8974	151.1788	195.3323
			$\omega_{N,r}$		61.2050	82.7747	127.5324	176.0205
		FEM	$\omega_{N,r}/\omega_{0,r}$		0.6325	0.7332	0.8436	0.9011
		Ref. [31]		—	0.6325	0.7300	0.8400	—

[a] $\omega_{0,r}$ = rth natural frequency of the pipe without axial load (i.e. $N = 0$),

[b] $\omega_{N,r}$ = rth natural frequency of the pipe with axial load $N = 0.6P_{1,cr}$.

3.1.2 *Stability Analysis of the 1-Span C-F Pipe*

The dimensions and physical properties of this 1-span cantilevered pipe are the same as those for Table 1 and its stability curve is shown in Figure 3(a) with ordinate denoting the dimensionless critical flow velocity U_{cr}^* and abscissa denoting the mass ratio m_f^*. Besides, Figure 3(b) shows the relationship between dimensionless critical frequency $(\lambda_{r,I})_{cr}$ and mass ratio m_f^*. In the two figures, the solid curves (——) are obtained from the presented FEM, and the dotted curves (……) are obtained from [32] for the C-F fluid-conveying pipe in air (with $\rho_w = 0$). Good agreement between the solid curves and dotted curves confirms the availability of the presented FEM and the developed computer program for this paper.

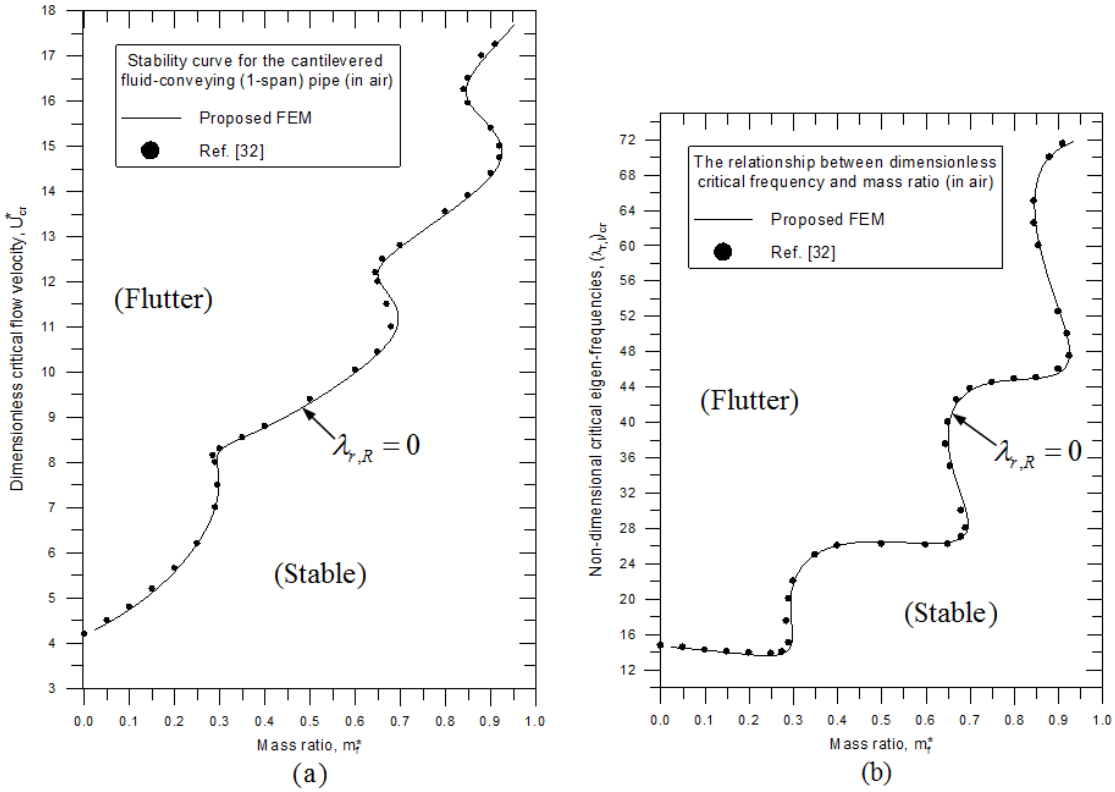

Figure 3: The Relationships between (a) The Dimensionless Critical Flow Velocity U^*_{cr} and Mass Ratio m^*_f, and (b) The Dimensionless Critical Frequency $(\lambda_{r,I})_{cr}$ and Mass Ratio m^*_f, for the 1-Span Cantilevered Fluid-Conveying Pipe in Air

3.2 Stability Analyses of the 1- to 4- Span Pipes

For convenience, in the subsequent subsections, the span lengths ℓ_i ($i=1$ to q) for each multi-span pipe are assumed to be equal to each other with $\ell_i=\ell_o=6.0$ m, and the flow velocity and eigenfrequency refer to the "dimensionless" ones, respectively, unless particularly mentioned. The Argand diagrams for the 1- to 4- span pipes (cf. Figure 2(a)-(d)) with three BCs are studied in this subsection: P-P, C-C and C-P. According to Timoshenko and Gere [30], a beam will be not operated normally after the onset of its first-mode buckling, thus, in practice, the information regarding the first-mode buckling is most significant. However, for comparisons, the higher critical flow velocity $U^*_{r,cr}$ associated with the *r*th complex eigenvalues ($r=1,2$) of each fluid-conveying pipe is also studied in addition to the first one $U^*_{1,cr}$. It is noted that, in the Argand diagrams shown in Figure 4 (for P-P pipes), 7 (for C-C pipes) and 10 (for C-P pipes), the digit nearby each symbol ● (regarding first eigenvalue) or ✖ (regarding second eigenvalue) denotes the associated value of flow velocity U^* and the spacing between any two adjacent symbol points is $\Delta U^*=0.2$ except for the first spacing to be $\Delta U^*=0.05$ (from $U^*=0.05$ to 0.1). Besides, some symbols are introduced: (i) The *r*th critical flow velocity of a fluid-conveying pipe (with $P_p=p_f A_f=0$ and $U\neq 0$) is denoted by ${}^{(q)}_{S}U^*_{r,cr}$ and the associated "buckled" mode shape by ${}^{(q)}_{S}\hat{Y}_r(x)$ with the left superscript "*q*" denoting the total number of *spans* for the entire pipe and the left subscript "S" denoting the *supporting* conditions. For example, ${}^{(3)}_{PP}\hat{Y}_1(x)$ denotes the 1st buckled mode shape of a 3-span P-P

pipe. If only *one* critical flow velocity is associated with the first (or second) complex eigenvalues, then it is denoted by $U^*_{1,cr}$ (or $U^*_{2,cr}$). However, if the total number of critical flow velocities associated with the first (or second) complex eigenvalues is greater than one, then they are denoted by $U^*_{1a,cr}$, $U^*_{1b,cr}$, $U^*_{1c,cr}$, … for those associated with the 1st complex eigenvalues and by $U^*_{2a,cr}$, $U^*_{2b,cr}$, $U^*_{2c,cr}$, … for those associated with the 2nd complex eigenvalues. (ii) The "equivalent" *r*th critical flow velocity for a classical axial-loaded "1-span" *beam* (with axial load $N = m_f V^2$) obtained from theory of *static* stability [30] is denoted by ${}_S V^*_{r,cr}$ and the corresponding "buckled" mode shape is denoted by ${}_S \hat{Z}_{r,cr}(x)$ as one may see from Eqs. (A.4), (A.5), (A.10), (A.11), (A.16) and (A.17) in the ***Appendix*** at the end of this paper. It is noted that U^* and $\hat{Y}$ (obtained from *dynamic* stability) are replaced by V^* and $\hat{Z}$ (obtained from *static* stability), respectively, to avoid confusion. Furthermore, the left superscript "(*q*)" is also removed from V^* and $\hat{Z}$, because, based on the theory of *static* stability for the buckling of a classical axial-loaded *beam* [30], only the values of V^* and $\hat{Z}$ for "1-span" *beams* ($q = 1$) can be obtained.

3.2.1 *With P-P end Supports (or BCs)*

The coordinates ($\lambda_{1,R}$, $\lambda_{1,I}$) and ($\lambda_{2,R}$, $\lambda_{2,I}$) for some relevant points on the loci of the 1st and 2nd complex eigenvalues of the 1-span fluid-conveying P-P pipe are listed in Table 2, and the associated Argand diagrams for the 1-, 2-, 3- and 4- span ones are shown in Figure 4 (a-1) and (a-2), (b-1) and (b-2), (c-1) and (c-2), and (d-1) and (d-2), respectively. In the latter figures, "Figure 4(*q*-*r*)" denotes the Argand diagram of the "*q*-span" pipe associated with the "*r*th" complex eigenvalues for various flow velocities ${}^{(q)}_{PP}U^*_r$, with *span number* $q = a = 1$, $q = b = 2$, $q = c = 3$, $q = d = 4$ and $r = 1,2$. For example, "Figure 4(b-1)" denotes the Argand diagram for the 2-span pipe associated with the 1st complex eigenvalues for flow velocities ${}^{(2)}_{PP}U^*_1 = 0.05 - 11.0$. From Table 2 and Figure 4(a-1) one sees that there are three critical flow velocities to be associated with the 1st complex eigenvalues λ_1: ${}^{(1)}_{PP}U^*_{1a,cr} = 3.1416 \approx \pi$, ${}^{(1)}_{PP}U^*_{1b,cr} = 6.2831 \approx 2\pi$ and ${}^{(1)}_{PP}U^*_{1c,cr} = 9.4118 \approx 3\pi$. If the flow velocity ${}^{(1)}_{PP}U^*_1$ is greater than the 1st or the 3rd critical ones, i.e., ${}^{(1)}_{PP}U^*_1 > {}^{(1)}_{PP}U^*_{1a,cr}$ or ${}^{(1)}_{PP}U^*_1 > {}^{(1)}_{PP}U^*_{1c,cr}$, the 1st frequency $\lambda_{1,I}$ will be equal to zero (i.e., $\lambda_{1,I} = 0$) and the pipe will be buckled, however, for the flow velocity ${}^{(1)}_{PP}U^*_1$ to be greater than the 2nd critical one ${}^{(1)}_{PP}U^*_{1b,cr}$ and less than the 3rd critical one ${}^{(1)}_{PP}U^*_{1c,cr}$, i.e., ${}^{(1)}_{PP}U^*_{1b,cr} < {}^{(1)}_{PP}U^*_1 < {}^{(1)}_{PP}U^*_{1c,cr}$, Table 2 and Figure 4(a-1) and (a-2) reveal that $\lambda_{1,I} = \lambda_{2,I}$ and $\lambda_{1,R} = -\lambda_{2,R}$, this result indicates that, in the last velocity range, the pipe will perform first-and-second-mode-coupled oscillations after it restores stability from its buckled state at the 2nd critical flow velocity ${}^{(1)}_{PP}U^*_{1b,cr}$. For convenience, the flow velocities ${}^{(1)}_{PP}U^*_r$ ($r = 1,2$) associated with the 1st and 2nd complex eigenvalues in the last velocity range, ${}^{(1)}_{PP}U^*_{1b,cr} < {}^{(1)}_{PP}U^*_r < {}^{(1)}_{PP}U^*_{1c,cr}$, are denoted by ${}^{(1)}_{PP}U^*_{1,coupled}$ and ${}^{(1)}_{PP}U^*_{2,coupled}$, respectively.

In other words, according to Table 2 and Figure 4 (a-1) and (a-2), the value of $\lambda_{1,I}$ (i.e., the first natural frequency of the pipe) decreases with the increase of the flow velocity ${}^{(1)}_{PP}U^*_1$ and approaches zero when ${}^{(1)}_{PP}U^*_1 \approx \pi$, which is the first

critical flow velocity denoted by ${}^{(1)}_{PP}U^*_{1a,cr}$ for buckling of the 1-span P-P pipe. After that, the values of $\lambda_{1,I}$ are equal to zero until ${}^{(1)}_{PP}U^*_1 \approx 2\pi$, which is the second critical flow velocity ${}^{(1)}_{PP}U^*_{1b,cr}$, and for the value of ${}^{(1)}_{PP}U^*_1$ greater than 2π and less than 3π, i.e., $2\pi < {}^{(1)}_{PP}U^*_1 < 3\pi$, the locus of the first eigenvalues (denoted by symbols ●) and that of the second eigenvalues (denoted by symbols ✖) combine on the vertical imaginary-axis (for $\lambda_{1,I}$ and $\lambda_{2,I}$) when ${}^{(1)}_{PP}U^*_1 \approx 6.3$ and then the loci leave the imaginary-axis at symmetric points, this indicates the onset of coupled-mode flutter [3].

Table 2: The Coordinates ($\lambda_{r,R}$, $\lambda_{r,I}$) for Some Relevant Points on the Loci of the 1st and 2nd Complex Eigen Values (for Various Flow Velocities ${}^{(1)}_{PP}U^*_r = 0.05 - 11.0$) of the 1-Span Fluid-Conveying P-P Pipe

${}^{(1)}_{PP}U^*_r$		**0.05**		**3.1415**	**3.1416** ${}^{(1)}_{PP}U^*_{1a,cr}$	…	**6.2831** ${}^{(1)}_{PP}U^*_{1b,cr}$	**6.2832**	**6.4**	…	**9.4117**	**9.4118** ${}^{(1)}_{PP}U^*_{1c,cr}$	**9.6**	…	**11.0**
λ_1	$\lambda_{1,R}$	0	0	0	**0.048**	…	**0.184**	0	**6.411**	…	10.876	**1.141**	-1.554	…	-1.885
	$\lambda_{1,I}$	9.868	…	0.072	**0**	0	**0**	0.116	**8.218**	…	0.231	**0**	0	0	0
λ_2	$\lambda_{2,R}$	0	0	0	0	0	0	0	**-6.411**	…	-10.876	-1.105	-9.655	…	28.652
	$\lambda_{2,I}$	39.477	…	34.800	34.799	…	9.912	9.905	**8.218**	…	0.231	0	25.028	…	29.832

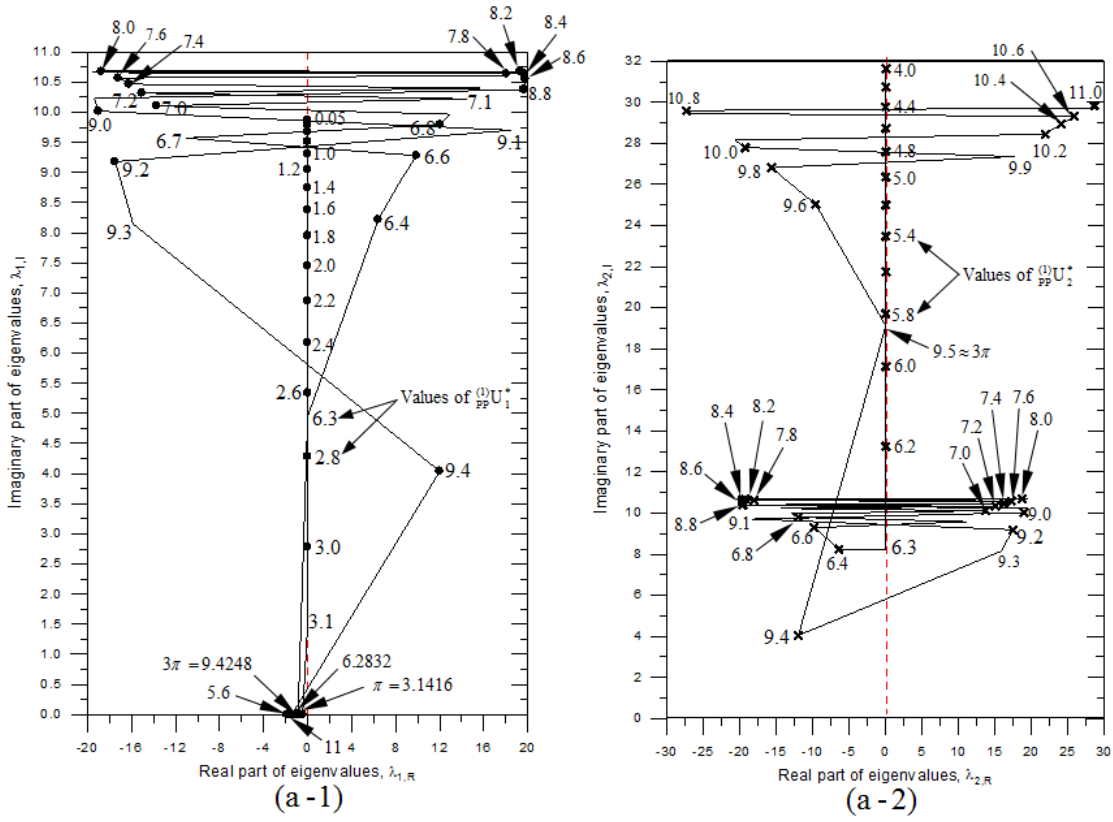

Figure 4: The Argand Diagrams for the 1st and 2nd Complex Eigen values of (a) 1-, (b) 2-, (c) 3- and (d) 4- Span Fluid-Conveying "P-P" pipes shown in Figure 2 (a)-(d) with Mass Ratio $m^*_f = 0.5$. In other words, (a-1) and (a-2) are Those of *1-Span* Pipe; (b-1) and (b-2) are Those of *2-Span* Pipe; (c-1) and (c-2) are Those of *3-Span* Pipe; and (d-1) and (d-2) are those of *4-Span* Pipe

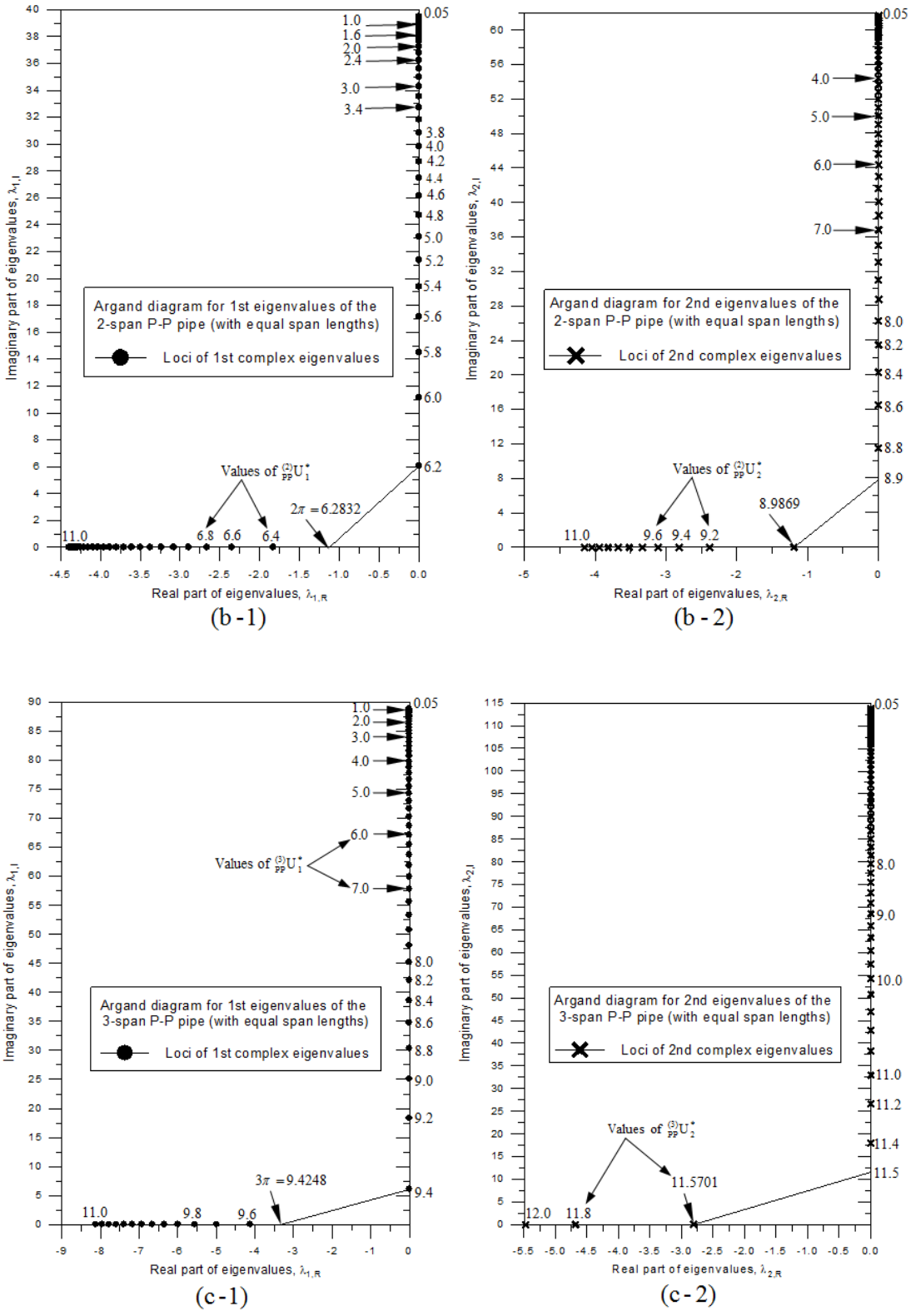

Figure 4: (Continued)

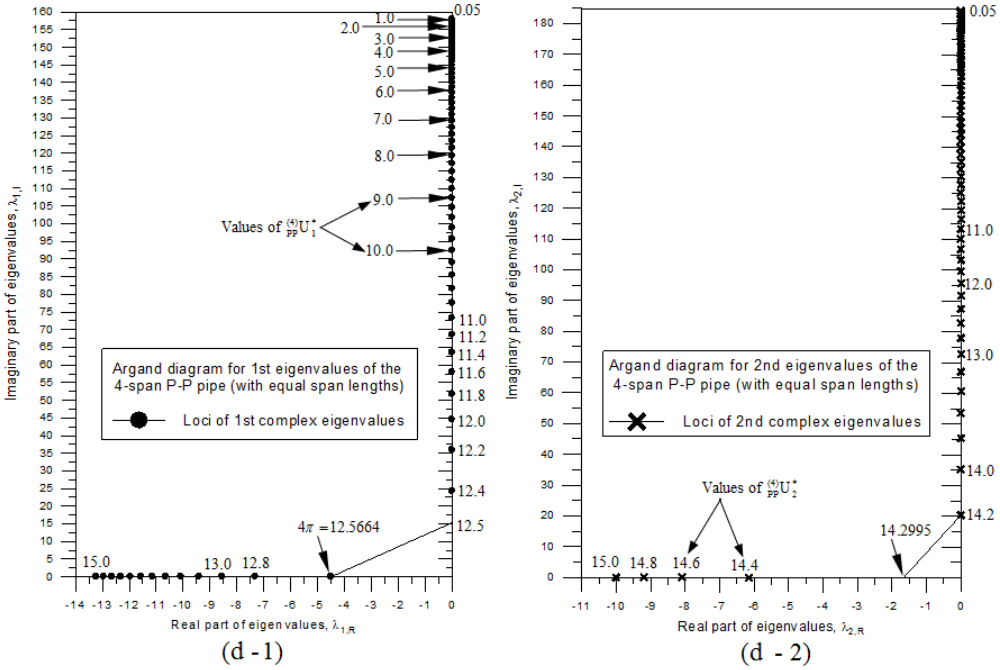

Figure 4: (Continued)

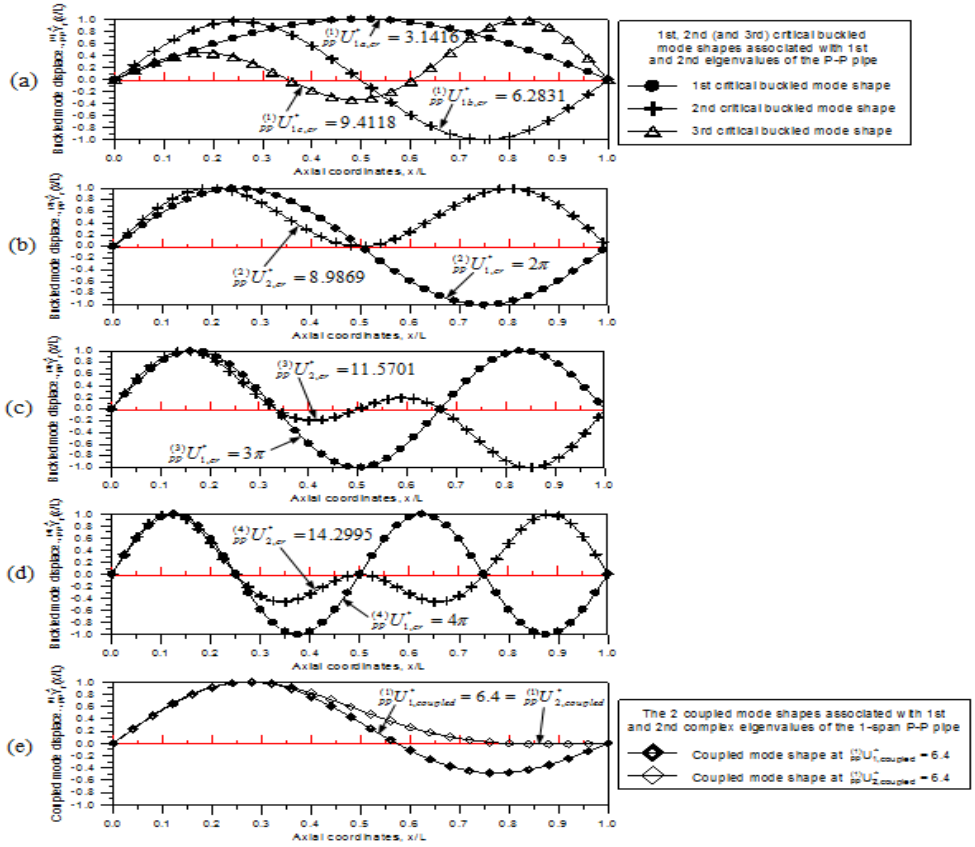

Figure 5: The first to Third Critical Buckled Mode Shapes for the (a) 1-, (b) 2-, (c) 3- and (d) 4- Span Fluid-Conveying "P-P" Pipes with Mass ratio $m^*_f = 0.5$, and (e) the "coupled" Mode Shapes of the 1-span P-P Pipe at Flow Velocity $^{(1)}_{PP}U^*_{1,coupled} = {}^{(1)}_{PP}U^*_{2,coupled} = 6.4$.

It is noted that, on the horizontal real ($\lambda_{1,R}$) axis of Figure 4(a-1), the space from $\lambda_{1,R} \approx -0.457$ to -1.885 is very small so that many symbols (●) in that space overlap each other.

The Argand diagrams associated with the 1st and 2nd eigenvalues of the 2-, 3- and 4- span P-P pipes shown in Figure 4(b-1) and (b-2), (c-1) and (c-2), and (d-1) and (d-2) are much simpler than those of the 1-span pipe shown in Figure 4(a-1) and (a-2). From Figure 4(b-1)-(d-2) one sees that the first-mode motion is not coupled with the second-mode motion, and the values of $\lambda_{1,I}$ decrease with the increase of ${}^{(q)}_{PP}U^*_1$ and equal to zero when ${}^{(q)}_{PP}U^*_1 \geq q\pi$ with $q = 2,3,4$. Thus, the first critical flow velocities for the 2-, 3- and 4- span fluid-conveying P-P pipes are 2π, 3π and 4π, respectively. This is a reasonable result, because the "first" critical buckled mode shapes ${}^{(q)}_{PP}\hat{Y}_1(\xi)$ (denoted by the curves —●—, with $\xi = x/L$) of the 2-, 3- and 4- span fluid-conveying pipes (based on ${}^{(q)}_{PP}U^*_{1,cr} = q\pi$ and $\lambda_{1,I} = 0$) shown in Figure 5 (b), (c) and (d), respectively, take the same forms as the second, third and fourth buckled mode shapes ${}_{PP}\hat{Z}_{r,cr}(\xi)$ (with $r = 2,3,4$) of the classical axial-loaded "1-span" P-P *beam* shown in Figure A.1(a) (in ***Appendix***) with its *r*th *equivalent* critical flow velocity of buckling given by ${}_{PP}V^*_{r,cr} = r\pi$ (with $r = 2,3,4$) as one may see from Eq. (A.4) (in ***Appendix***).

It is noted that the two coupled *mode shapes* for the 1-span P-P pipe associated with the same flow velocities ${}^{(1)}_{PP}U^*_{1,coupled} = {}^{(1)}_{PP}U^*_{2,coupled} = 6.4$ shown in Figure 5(e) are not identical, because a mode shape is dependent on its eigenvalue λ_r and, at ${}^{(1)}_{PP}U^*_{1,coupled} = {}^{(1)}_{PP}U^*_{2,coupled} = 6.4$, the *real* part of the 1st eigenvalue λ_1 is "opposite" to that of the 2nd eigenvalue λ_2, i.e., $\lambda_{1,R} = 6.411 = -\lambda_{2,R}$, in spite of the fact that the *imaginary* parts of the last two eigenvalues are equal to each other (i.e., $\lambda_{1,I} = \lambda_{2,I} = 8.218$) as one may see from column 10 of Table 2.

3.2.2 *With C-C end supports (or BCs)*

For the C-C BCs, the configurations of the 1- to 4- span fluid-conveying pipes with equal span lengths $\ell_o = 6\,\text{m}$ are shown in Figure 6 and the Argand diagrams associated with the 1st and 2nd complex eigenvalues of the "*q*-span" pipe are shown in Figure 7(*q*-1) and (*q*-2), respectively, with *span number* $q = a = 1$, $q = b = 2$, $q = c = 3$ and $q = d = 4$. The coordinates ($\lambda_{1,R}$, $\lambda_{1,I}$) and ($\lambda_{2,R}$, $\lambda_{2,I}$) for some relevant points on the loci of the 1st and 2nd complex eigenvalues of the 1-span and 3-span C-C pipe are listed in Tables 3(a) and (b), respectively. From Table 3(a) and Figure 7(a-1) one sees that all the three critical flow velocities, ${}^{(1)}_{CC}U^*_{1a,cr} = 6.2832 \approx 2\pi$, ${}^{(1)}_{CC}U^*_{1b,cr} = 8.9868$ and ${}^{(1)}_{CC}U^*_{1c,cr} = 12.5665 \approx 4\pi$, are associated with the 1st eigenvalues λ_1 and have nothing to do with the 2nd eigenvalues λ_2. From the corresponding buckled mode shapes ${}^{(1)}_{CC}\hat{Y}_r(\xi)$ shown in Figure 8(a) one sees that the 1st one ${}^{(1)}_{CC}\hat{Y}_1(\xi)$ and the 3rd one ${}^{(1)}_{CC}\hat{Y}_3(\xi)$, take the same form as the first and second buckled mode shapes of the classical axial-loaded "1-span" C-C *beam* with $N = m_f V^2$, ${}_{CC}\hat{Z}_{1,cr}(\xi)$ and ${}_{CC}\hat{Z}_{2,cr}(\xi)$, respectively, shown in Figure A.1(b) (in ***Appendix***). Since the "equivalent" critical flow velocities corresponding to ${}_{CC}\hat{Z}_{1,cr}(\xi)$ and ${}_{CC}\hat{Z}_{2,cr}(\xi)$ are given by Eq. (A.10): ${}_{CC}V^*_{1,cr} = 2\pi$ and ${}_{CC}V^*_{2,cr} = 4\pi$, the 1st and 3rd critical flow velocities of the *pipe* are given by ${}^{(1)}_{CC}U^*_{1a,cr} \approx 2\pi = {}_{CC}V^*_{1,cr}$ and ${}^{(1)}_{CC}U^*_{1c,cr} \approx 4\pi = {}_{CC}V^*_{2,cr}$ as shown in Table 3(a)

and Figure 7(a-1). From the last table and figure, one sees that, the pipe will be "buckled" if the flow velocity ${}_{CC}^{(1)}U_1^*$ (associated with the 1st complex eigenvalues λ_1) is greater than the 1st critical flow velocity (${}_{CC}^{(1)}U_1^* > {}_{CC}^{(1)}U_{1a,cr}^*$) or 3rd one (${}_{CC}^{(1)}U_1^* > {}_{CC}^{(1)}U_{1c,cr}^*$), and will restore stability and coupled with the oscillation (or flutter) associated with the 2nd complex eigeanvalyes λ_2 if ${}_{CC}^{(1)}U_1^*$ is grater than the 2nd critical flow velocity and less than the 3rd one (${}_{CC}^{(1)}U_{1b,cr}^* < {}_{CC}^{(1)}U_1^* < {}_{CC}^{(1)}U_{1c,cr}^*$).

For the classical axial-loaded "1-span" C-C *beam*, its *r*th critical buckled mode shape is determined by Eq. (A.11), i.e. ${}_{CC}\hat{Z}_{r,cr}(x) = \overline{A}_r(1-\cos\alpha_r x)$. Since $|\cos\alpha_r x| \le 1.0$, the magnitude of the last mode shape is greater than or equal to zero (i.e., ${}_{CC}\hat{Z}_{r,cr}(x) \ge 0$) as one may see from Figure A.1(b). This is the reason why the mode shape ${}_{CC}^{(1)}\hat{Y}_2(\xi)$ corresponding to the 2nd critical flow velocity ${}_{CC}^{(1)}U_{1b,cr}^* = 8.9868$ does not appear in Figure A.1(b) for the classical axial-loaded "1-span" C-C *beam*. It is noted that the Argand diagrams shown in Figure 7 are based on Eq. (17), in which, the overall effective damping matrix $[\bar{c}]$ is obtained from the assembly of the element damping matrix $[c]_e$ given by Eqs. (13) and (15a) with Coriolis force as the matrix coefficients for the case of $\hat{E} = C_o = 0$. Thus, the mode shape ${}_{CC}^{(1)}\hat{Y}_2(\xi)$ corresponding to the 2nd critical flow velocity ${}_{CC}^{(1)}U_{1b,cr}^* = 8.9868$ is due to the Coriolis effect and this effect should be the mechanism for the pipe restoring stability and coupling with the oscillation (or flutter) associated with the 2nd complex eigeanvalyes λ_2 if ${}_{CC}^{(1)}U_{1b,cr}^* < {}_{CC}^{(1)}U_1^* < {}_{CC}^{(1)}U_{1c,cr}^*$.

For the 2-span C-C pipe shown in Figure 6(b), the Argand diagrams associated with its 1st and 2nd complex eigenvalues are shown in Figure 7(b-1) and (b-2), respectively. From Figure 7(b-1) one sees that the 1st critical flow velocity is given by ${}_{CC}^{(2)}U_{1,cr}^* = 8.9869$ and the corresponding "buckled" mode shape (denoted by the curve —●—) is shown in Figure 8(b), which takes the same form for the 2nd buckled mode shape (cf. the curve —✚—) of the 1-span C-C pipe shown in Figure 8(a), i.e., ${}_{CC}^{(2)}\hat{Y}_1(\xi) \approx {}_{CC}^{(1)}\hat{Y}_2(\xi)$, thus, ${}_{CC}^{(2)}U_{1,cr}^* = 8.9869 \approx {}_{CC}^{(1)}U_{1b,cr}^*$, as they should be. Furthermore, from Figure 7(b-2) one sees that the 2nd critical flow velocity of the 2-span C-C pipe is given by ${}_{CC}^{(2)}U_{2,cr}^* = 4\pi$ with corresponding buckled mode shape shown in Figure 8(b). Because the last buckled mode shape ${}_{CC}^{(2)}\hat{Y}_2^*(\xi)$ takes the same form as the 2nd mode shape ${}_{CC}\hat{Z}_2(\xi)$ of the classical axial-loaded "1-span" C-C *beam* with ${}_{CC}V_{2,cr}^* = 4\pi$ as shown in Figure A.1(b), thus, ${}_{CC}^{(2)}U_{2,cr}^* = 4\pi = {}_{CC}V_{2,cr}^*$.

For the 3-span C-C pipe shown in Figure 6(c), the Argand diagrams associated with its 1st and 2nd complex eigenvalues are shown in Figs. 7(c-1) and (c-2), respectively, and the coordinates ($\lambda_{1,R}$, $\lambda_{1,I}$) and ($\lambda_{2,R}$, $\lambda_{2,I}$) for some relevant points on the loci of the 1st and 2nd eigenvalues are listed in Table 3(b). From Table 3(b) and Figure 7(c-1) and (c-2) one sees that the values of $\lambda_{1,I}$ and $\lambda_{2,I}$ decrease with the increase of flow velocity ${}_{CC}^{(3)}U_r^*$, and $\lambda_{1,I} = 0$ (but $\lambda_{2,I}$ = 105.12) when ${}_{CC}^{(3)}U_r^* = 11.5701$, which is the 1st critical buckling flow velocity ${}_{CC}^{(3)}U_{1a,cr}^*$ associated with the 1st eigenvalues. For the flow velocities greater than ${}_{CC}^{(3)}U_{1a,cr}^* = 11.5701$, $\lambda_{1,I} = 0$ and the value of $\lambda_{2,I}$ continuously decreases with the increase of ${}_{CC}^{(3)}U_r^*$, and both $\lambda_{1,I}$ and $\lambda_{2,I}$ are equal to zero ($\lambda_{1,I} = \lambda_{2,I} = 0$) when ${}_{CC}^{(3)}U_r^* = 15.4087$, which is the 1st critical

buckling flow velocity ${}^{(3)}_{CC}U^*_{2a,cr}$ associated with the 2nd eigenvales. For the flow velocities ${}^{(3)}_{CC}U^*_r$ to be greater than ${}^{(3)}_{CC}U^*_{2a,cr}=15.4087$, $\lambda_{1,I}=\lambda_{2,I}=0$ until ${}^{(3)}_{CC}U^*_r=17.3924$, which is the 2nd critical flow velocity associated with 1st and 2nd complex eigenvalues, i.e., ${}^{(3)}_{CC}U^*_{1b,cr}=17.3924={}^{(3)}_{CC}U^*_{2b,cr}$. Both the 1st-mode and 2nd-mode vibrations begin to couple when the flow velocity is greater than the last critical value. After that, the pipe restores stability with $\lambda_{1,I}=\lambda_{2,I}=0.073$ and $\lambda_{1,R}=87.435=-\lambda_{2,R}$, and $\lambda_{1,I}=0$ (but $\lambda_{2,I}$ = 15.968) when ${}^{(3)}_{CC}U^*_r=18.8496$, which is the 3rd critical buckling flow velocity ${}^{(3)}_{CC}U^*_{1c,cr}$ associated with the 1st eigenvalues. For the flow velocities to be greater than ${}^{(3)}_{CC}U^*_{1c,cr}=18.8496$, $\lambda_{1,I}=0$ and $\lambda_{2,I}$ continuously decreases with the increase of ${}^{(3)}_{CC}U^*_r$, and both $\lambda_{1,I}$ and $\lambda_{2,I}$ are equal to zero (i.e., $\lambda_{1,I}=\lambda_{2,I}=0$) when ${}^{(3)}_{CC}U^*_r=21.7891$, which is the 3rd critical buckling flow velocity ${}^{(3)}_{CC}U^*_{2c,cr}$ associated with the 2nd eigenvalues. For comparison, the buckled mode shapes corresponding to the two critical flow velocities (${}^{(3)}_{CC}U^*_{1a,cr}=11.5701$ and ${}^{(3)}_{CC}U^*_{1b,cr}=17.3924$) associated with the 1st eigenvales λ_1 and those (${}^{(3)}_{CC}U^*_{2a,cr}=15.4087$ and ${}^{(3)}_{CC}U^*_{2b,cr}=17.3924$) associated with the 2nd eigenvales λ_2 are plotted in Figure 8(c). It is seen that the mode displacements of all the four buckled mode shapes are in the range from +1.0 to -1.0, i.e., $-1.0\le {}^{(3)}_{CC}\hat{Y}_r(\xi)\le+1.0$, instead of greater than or equal to zero for the buckled mode shapes of the classical axial-loaded "1-span" C-C *beam* (${}_{CC}\hat{Z}_r(x)\ge 0$) shown in Figure A.1(b). For the last reason, the foregoing critical buckling flow velocities of the 3-span C-C *pipe* are not equal to $2r\pi$ (i.e., ${}^{(3)}_{CC}U^*_{r,cr}\neq 2r\pi$), with $r=1,2,3,\ldots$.

For the 4-span C-C pipe shown in Figure 6(d), from the Argand diagrams associated with its 1st and 2nd eigenvalues shown in Figure 7(d-1) and (d-2), one sees that the pipe will be buckled when ${}^{(4)}_{CC}U^*_r=14.2995$, which is the 1st critical buckling flow velocity ${}^{(4)}_{CC}U^*_{1,cr}$ associated with the 1st eigenvalues λ_1. For the flow velocities to be greater than ${}^{(4)}_{CC}U^*_{1,cr}=14.2995$, $\lambda_{1,I}$ is always equal to zero ($\lambda_{1,I}\equiv 0$) and $\lambda_{2,I}$ decreases with the increase of ${}^{(4)}_{CC}U^*_r$, and $\lambda_{2,I}=0$ when ${}^{(4)}_{CC}U^*_r=17.9737$, which is the 2nd critical buckling flow velocity associated with the 2nd eigenvalues, i.e., ${}^{(4)}_{CC}U^*_{2a,cr}=17.9737$. From the Argand diagram shown in Figure 7(d-2), it is seen that the pipe will restore stability at ${}^{(4)}_{CC}U^*_{2b,cr}=23.5108$ and be buckled again at ${}^{(4)}_{CC}U^*_{2c,cr}=25.1330\approx 8\pi$. It is different from the first-and-second-mode-coupled vibrations of the 3-span C-C pipe (cf. Figure 7(c-1) and (c-2)) that the vibration of the 4-span C-C pipe is associated with the 2nd eigenvalues only "after it restores stability" at ${}^{(4)}_{CC}U^*_{2b,cr}=23.5108$. The 1st, 2nd and 4th buckled mode shapes of the 4-span C-C pipe are shown in Figure 8(d). It is seen that the 4th buckled mode shape of the 4-span C-C *pipe* takes the same form as the 4th one of the classical axial-loaded "1-span" C-C *beam* shown in Figure A.1(b), thus, the corresponding critical flow velocity ${}^{(4)}_{CC}U^*_{2c,cr}$ is equal to ${}_{CC}V^*_{4,cr}$, i.e., ${}^{(4)}_{CC}U^*_{2c,cr}\approx 8\pi={}_{CC}V^*_{4,cr}$

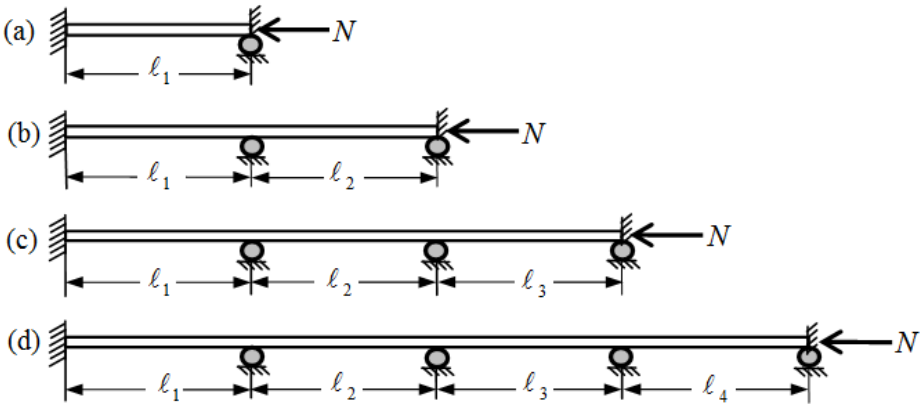

Figure 6: The Four Uniform Fluid-Conveying C-C Pipes Subjected to Axial load $N = m_f U^2$ with Equal Span Lengths $\ell_1 = \ell_2 = \ell_3 = \ell_4 = \ell_0$. The Other Legends are the Same as Those of Figure 2.

Table 3: The Coordinates ($\lambda_{r,R}$, $\lambda_{r,I}$) for Some Points on the Loci of the 1st and 2nd Eigen Values of the C-C Pipes

(a) For 1-span C-C pipe

	$_{CC}^{(1)}U_r^*$	**0.05**	**…**	**6.2831**	**6.2832** $_{CC}^{(1)}U_{1a,cr}^*$	**…**	**8.9868** $_{CC}^{(1)}U_{1b,cr}^*$	**8.9869**	**9.2**	**9.3**	**…**	**12.2**	**12.3**	**12.5664**	**12.5665** $_{CC}^{(1)}U_{1c,cr}^*$	**…**	**15.0**
λ_1	$\lambda_{1,R}$	0	0	0	**0.067**	…	**0.105**	0	0	1.408	…	7.422	0	0	**0.183**		1.556
	$\lambda_{1,I}$	22.372	…	0.098	**0**	0	**0**	0.161	10.567	17.095	…	27.173	19.335	0.068	**0**	0	0
λ_2	$\lambda_{2,R}$	0	0	0	0	0	0	0	0	-1.408	…	-7.422	8.130	17.646	17.649	…	-30.460
	$\lambda_{2,I}$	61.672	…	47.496	47.495	…	26.982	26.980	22.682	17.095	…	27.173	40.149	43.518	43.519	…	56.355

.

(b) For 3-span C-C pipe

	$_{CC}^{(3)}U_r^*$	**0.05**	**…**	**11.5700**	**11.5701** $_{CC}^{(3)}U_{1a,cr}^*$	**…**	**15.4086**	**15.4087** $_{CC}^{(3)}U_{2a,cr}^*$	**…**	**17.3924 #**	**17.3925**	**…**	**18.8495**	**18.8496** $_{CC}^{(3)}U_{1c,cr}^*$	**…**	**21.7890**	**21.7891** $_{CC}^{(3)}U_{2c,cr}^*$	**…**	**22.0**
λ_1	$\lambda_{1,R}$	0	0	0	**0.191**	…	9.377	9.337	…	**9.566**	87.435	…	0	**0.604**	…	9.482	9.482	⋯	9.602
	$\lambda_{1,I}$	113.83	…	0.436	**0**	0	0	0	0	**0**	0.073	…	0.42	**0**	0	0	0	0	0
λ_2	$\lambda_{2,R}$	0	0	0	0	0	0	**-0.337**	…	**-9.552**	-87.435	…	-100.54	100.543	…	0	**-1.863**	…	-9.41
	$\lambda_{2,I}$	166.22	…	105.12	105.12	…	0.545	**0**	0	**0**	0.073	…	15.967	15.968	…	2.874	**0**	0	0

.# $_{CC}^{(3)}U_{1b,cr}^* = {}_{CC}^{(3)}U_{2b,cr}^*$

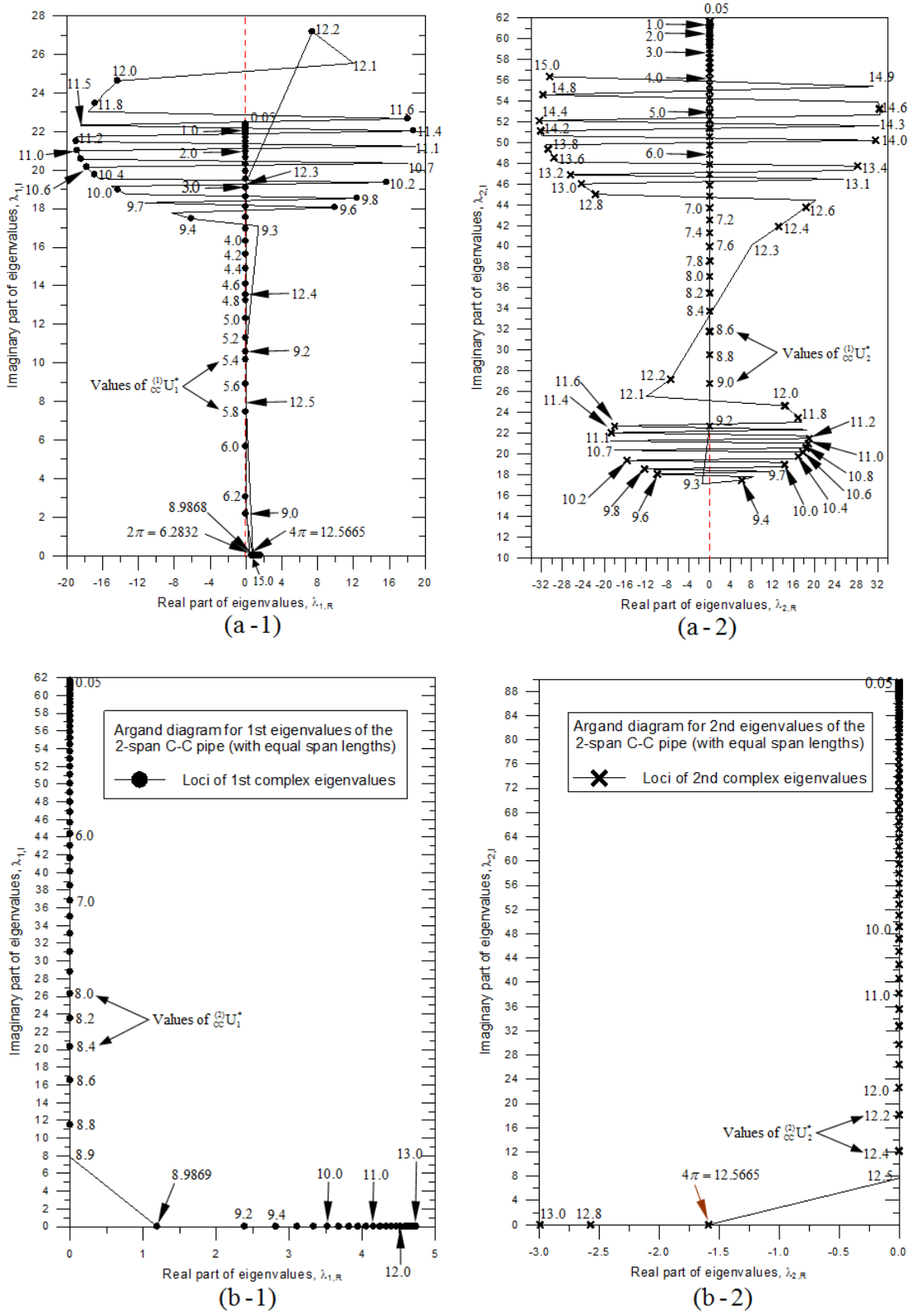

Figure 7: The Argand diagrams for the 1st and 2nd complex eigenvalues of (a) 1-, (b) 2-, (c) 3- and (d) 4- span fluid-conveying C-C pipes shown in Figs. 6(a)-(d) with mass ratio $m_f^* = 0.5$. In other words, (a-1) and (a-2) are those of *1-span* pipe; (b-1) and (b-2) are those of *2-span* pipe; (c-1) and (c-2) are those of *3-span* pipe; and (d-1) and (d-2) are those of *4-span* pipe.

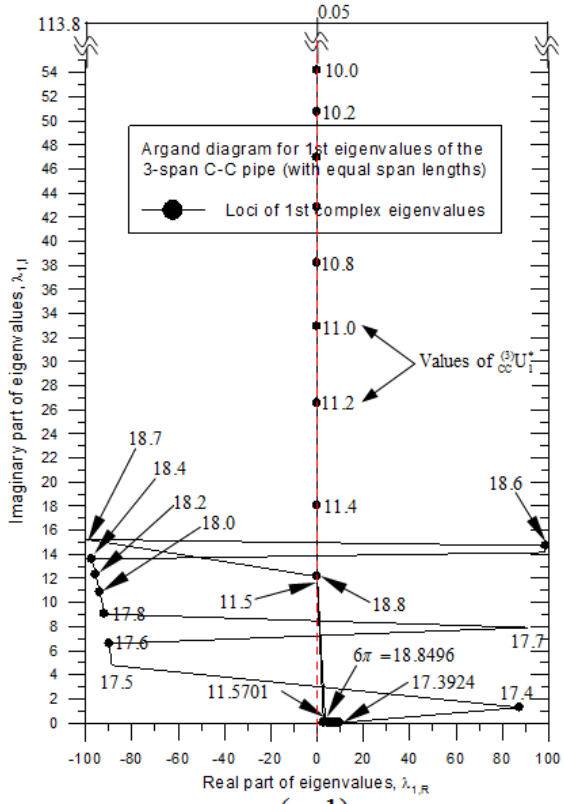

(c - 1)

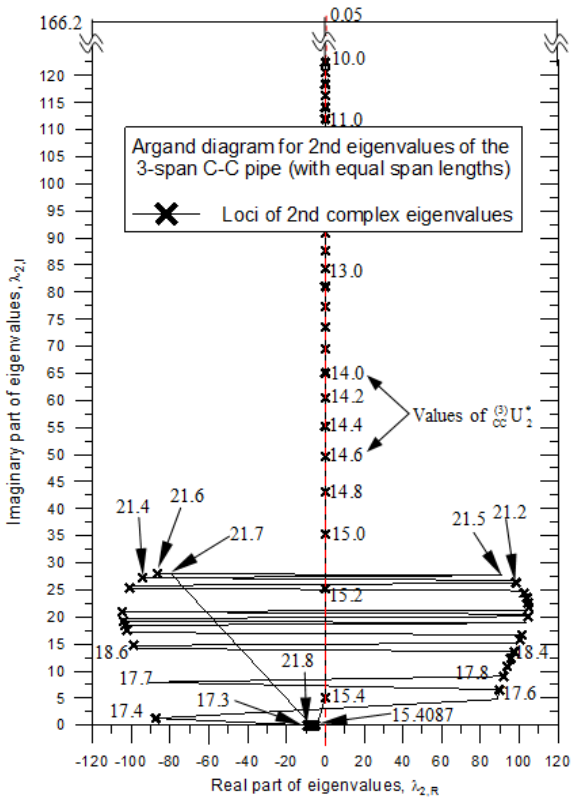

(c - 2)

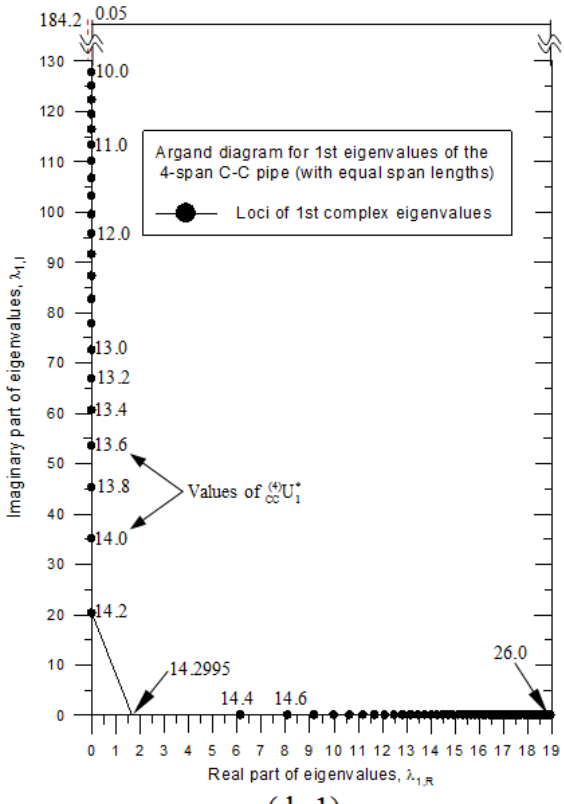

(d - 1)

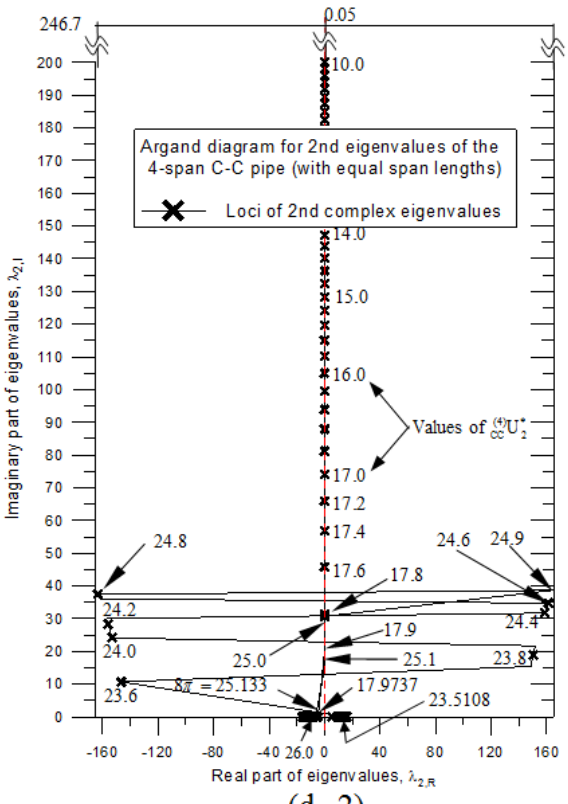

(d - 2)

Figure 7: (Continued)

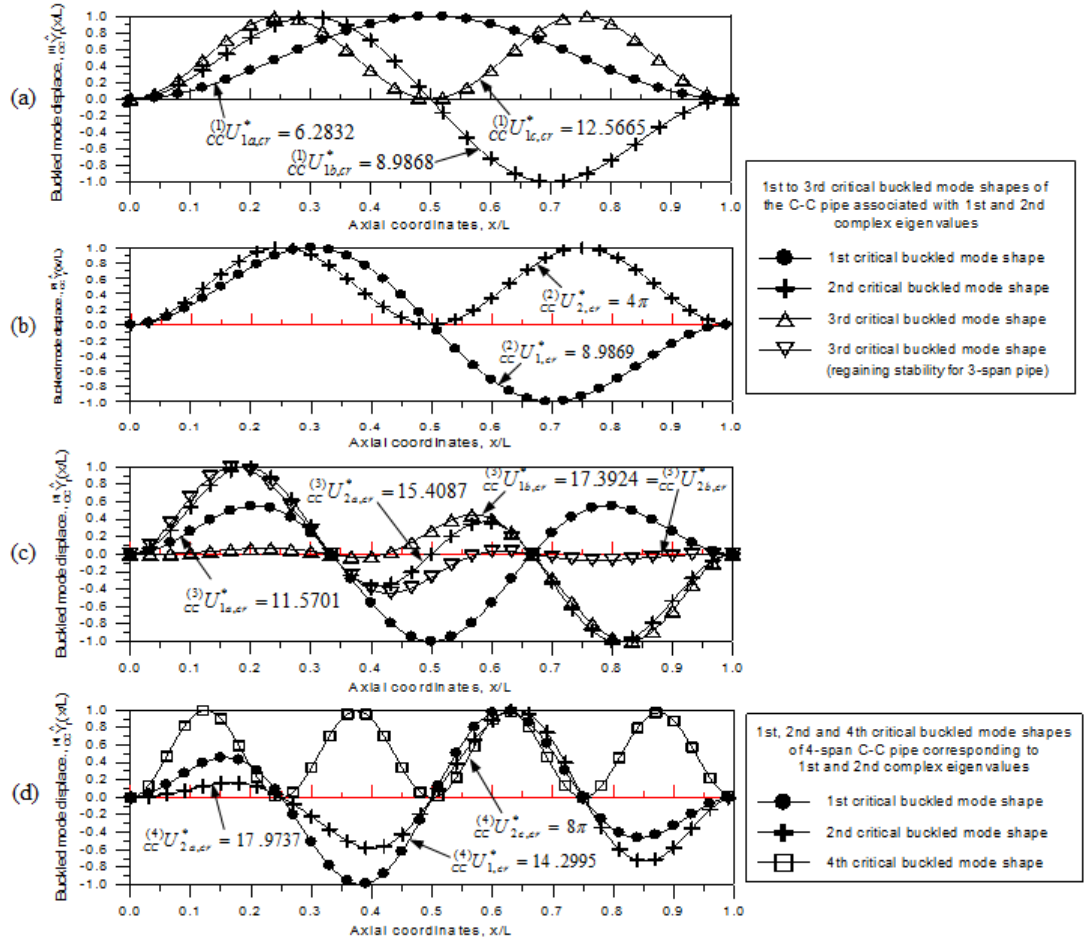

Figure 8 The 1st to 4th "buckled" Mode Shapes of (a) 1-, (b) 2-, (c) 3- and (d) 4- span Fluid-Conveying C-C pipes Shown in Figure 6(a)-(d) with Mass Ratio $m^*_f = 0.5$.

3.2.3 *With C-P end supports (or BCs)*

The configurations of the 1- to 4- span fluid-conveying C-P pipes with equal span lengths $\ell_o = 6$ m are shown in Figure 9 and the Argand diagrams associated with the 1st and 2nd complex eigenvalues of the *q*-span pipes are shown in Figure 10(*q*-1) and (*q*-2), respectively, with *span number* $q = a = 1$, $q = b = 2$, $q = c = 3$ and $q = d = 4$. The coordinates $(\lambda_{r,R}, \lambda_{r,I})$ for some relevant points on the loci of the *r*th eigenvalues (with $r = 1,2$) for the 1- and 2- span C-P pipes are shown in Tables 4(a) and (b), respectively. It is similar to the 1-span P-P pipe (Figure 4(a)) and the 1-span C-C pipe (Figure 7(a)) that all the lowest three critical flow velocities of the C-P pipe, $^{(1)}_{CP}U^*_{1a,cr} = 4.4935$, $^{(1)}_{CP}U^*_{1b,cr} = 7.7252$ and $^{(1)}_{CP}U^*_{1c,cr} = 10.9042$, are associated with the 1st eigenvalues and have nothing to do with the 2nd ones as one may see from Table 4(a) and Figure 10(a-1) and (a-2). The pipe will be buckled if the flow velocity $^{(1)}_{CP}U^*_1$ is greater than the 1st critical one ($^{(1)}_{CP}U^*_{1a,cr}$) or 3rd critical one ($^{(1)}_{CP}U^*_{1c,cr}$), and will regain stability if the value of $^{(1)}_{CP}U^*_r$ is greater than the 2nd critical flow velocity ($^{(1)}_{CP}U^*_{1b,cr}$). In addition, the vibration of the pipe is first-and-second-mode-coupled for the flow velocity $^{(1)}_{CP}U^*_1$ to be in the range of 2nd to 3rd critical ones, i.e., $^{(1)}_{CP}U^*_{1b,cr} \le {}^{(1)}_{CP}U^*_1 \le {}^{(1)}_{CP}U^*_{1c,cr}$. Since the corresponding three buckled mode

shapes shown in Figure 11(a) take the same forms as the lowest three ones of the classical axial-loaded "1-span" C-P *beam* shown in Figure A.1(c), one has: ${}^{(1)}_{CP}U^*_{1a,cr} = 4.4935 = {}_{CP}V^*_{1,cr}$, ${}^{(1)}_{CP}U^*_{1b,cr} = 7.7252 = {}_{CP}V^*_{2,cr}$, ${}^{(1)}_{CP}U^*_{1c,cr} = 10.9042 = {}_{CP}V^*_{3,cr}$.

For the 2-span C-P pipe, the coordinates $(\lambda_{r,R}, \lambda_{r,I})$ for some relevant points on the locus of the *r*th complex eigenvalue λ_r show in Table 4(b) and the Argand diagrams shown in Figure 10(b-1) and (b-2) reveal that the pipe will be buckled in 1st mode if the flow velocity ${}^{(2)}_{CP}U^*_r$ is greater than the 1st critical one ${}^{(2)}_{CP}U^*_{1a,cr} = 7.1498$ associated with the 1st eigenvalue λ_1 and in 2nd mode if the value of ${}^{(2)}_{CP}U^*_r$ is greater than the 2nd critical one ${}^{(2)}_{CP}U^*_{2a,cr} = 10.8852$ associated with the 2nd eigenvalue λ_2. The last two buckled modes will restore stability when ${}^{(2)}_{CP}U^*_r > 11.7554$, thus, 11.7554 is the 3rd critical flow velocity associated with both the 1st and 2nd eigenvalues, i.e., ${}^{(2)}_{CP}U^*_{1b,cr} = {}^{(2)}_{CP}U^*_{2b,cr} = 11.7554$. For the flow velocities to be greater than the last critical values, the 1st mode vibration and the 2nd one will be coupled. Since the 1st and 2nd buckled mode shapes shown in Figure 11(b) *look like* the 2nd and 3rd buckled mode shapes of the classical axial-loaded "1-span" C-P *beam* shown in Figure A.1(c) to some degree, respectively, the corresponding critical flow velocities ${}^{(2)}_{CP}U^*_{1a,cr} = 7.1498$ and ${}^{(2)}_{CP}U^*_{2a,cr} = 10.8852$ are somewhat close to ${}_{CP}V^*_{2,cr} = 7.7253$ and ${}_{CP}V^*_{3,cr} = 10.9041$, respectively.

For the 3-span C-P pipe, from its Argand diagrams shown in Figure 10(c-1) and (c-2) one sees that the pipe will be buckled in 1st mode if the flow velocity ${}^{(3)}_{CP}U^*_r$ is greater than the 1st critical one ${}^{(3)}_{CP}U^*_{1,cr} = 10.0379$ associated with the 1st eigenvalue λ_1 and in 2nd mode if the value of ${}^{(3)}_{CP}U^*_r$ is greater than the 2nd critical one ${}^{(3)}_{CP}U^*_{2,cr} = 13.4803$ associated with the 2nd eigenvalue λ_2. From the lowest two buckled mode shapes shown in Figure 11(c) one sees that the 1st one look like the 3rd buckled mode shapes for the classical axial-loaded "1-span" C-P beam shown in Figure A.1(c) to some degree, thus, the corresponding critical flow velocity ${}^{(3)}_{CP}U^*_{1,cr} = 10.0379$ is somewhat close to ${}_{CP}V^*_{3,cr} = 10.9041$.

For the 4-span C-P pipe with its Argand diagrams shown in Figure 10(d-1) and (d-2), it is seen that the 1st-mode buckling occurs when the flow velocity ${}^{(4)}_{CP}U^*_r$ is greater than the 1st critical one ${}^{(4)}_{CP}U^*_{1,cr} = 13.0366$ associated with the 1st eigenvalue λ_1 and the 2nd-mode buckling occurs when the value of ${}^{(4)}_{CP}U^*_r$ is greater than the 2nd critical one ${}^{(4)}_{CP}U^*_{2,cr} = 16.0408$ associated with the 2nd eigenvalue λ_2. Since the corresponding lowest two buckled mode shapes shown in Figure 11(d) are different from anyone of the lowest four buckled mode shapes for the classical axial-loaded "1-span" C-P *beam* shown in Figure A.1(c), the foregoing two critical flow velocities, ${}^{(4)}_{CP}U^*_{1,cr} = 13.0366$ and ${}^{(4)}_{CP}U^*_{2,cr} = 16.0408$, are not close to any of the *equivalent* ones, ${}_{CP}V^*_{r,cr}$ $(r = 1-4)$, given by Eqs. (A.16) and (A.19). However, since the 1st critical buckled mode shape of the 4-span C-P pipe shown in Figure 11(d), ${}^{(4)}_{CP}\hat{Y}_{1,cr}$, *looks like* the 4th buckled mode shape of the classical axial-loaded "1-span" P-P *beam* shown in Figure A.1(a), ${}_{PP}\hat{Z}_{4,cr}$, its critical flow velocity ${}^{(4)}_{CP}U^*_{1,cr} = 13.0366$ is slightly greater than ${}_{PP}V^*_{4,cr} = 4\pi = 12.56$, because the stiffness of the C-P pipe is slightly greater than that of the corresponding P-P pipe.

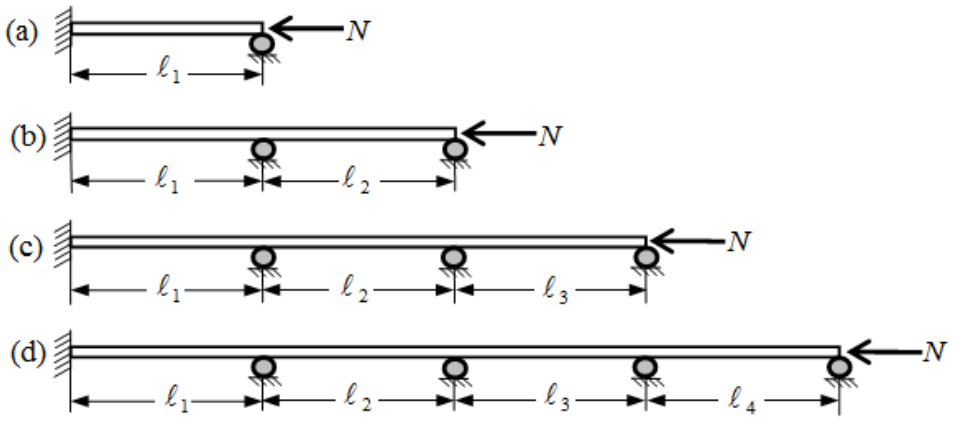

b

Figure 9: The Four Uniform Fluid-Conveying C-P Pipes Subjected to Axial Load $N = m_f U^2$ with Equal Span Lengths $\ell_1 = \ell_2 = \ell_3 = \ell_4 = \ell_0$. The Other Legends are the same as those of Figure 2

Table 4: The Coordinates ($\lambda_{r,R}$, $\lambda_{r,I}$) for Some Relevant Points on the Loci of the 1st and 2nd Complex Eigen Values of the Fluid-Conveying C-P Pipes: (a) 1-Span; (b) 2-Span

(a) 1-Span C-P Pipe

$_{CP}^{(1)}U_r^*$		**0.05**	**…**	**4.4934**	**4.4935** $_{CP}^{(1)}U_{1a,cr}^*$	**…**	**7.7252** $_{CP}^{(1)}U_{1b,c}^*$	**7.7253**	**7.9**	**8.0**	**…**	**10.7**	**10.8**	**10.9041**	**10.9042** $_{CP}^{(1)}U_{1c,cr}^*$	**…**	**12.0**
λ_1	$\lambda_{1,R}$	0	0	0	**0.102**	…	**0.159**	0	-7.598	9.655	…	15.887	12.637	0	**0.241**	…	1.802
	$\lambda_{1,I}$	15.417	…	0.029	**0**	0	**0**	0.197	11.170	11.756	…	15.162	14.966	0.397	**0**	0	0
λ_2	$\lambda_{2,R}$	0	0	0	0	0	0	0	7.598	-9.655	…	-15.887	-12.637	0	0	…	27.367
	$\lambda_{2,I}$	49.964	…	41.655	41.655	…	14.597	14.593	11.170	11.756	…	15.162	14.966	23.543	23.574	…	36.829

(b) 2-Span C-P Pipe

$_{CP}^{(2)}U_r^*$		**0.05**	**…**	**7.1497**	**7.1498** $_{CP}^{(2)}U_{1a,cr}^*$	**7.3**	**…**	**10.8851**	**10.8852** $_{CP}^{(2)}U_{2a,cr}^*$	**…**	**11.7554 #**	**11.7555**	**11.9**	**12.0**
λ_1	$\lambda_{1,R}$	0	0	0	**0.291**	2.023	…	4.354	4.354	…	**4.108**	36.311	-37.530	-38.299
	$\lambda_{1,I}$	46.055	…	0.135	**0**	0	0	0	0	…	**0**	0.123	4.712	6.031
λ_2	$\lambda_{2,R}$	0	0	0	0	0	0	0	**-0.307**	…	**-4.105**	-36.311	37.530	38.299
	$\lambda_{2,I}$	79.684	…	58.255	58.254	57.233	…	0.255	**0**	…	**0**	0.125	4.712	6.031

.# $_{CP}^{(2)}U_{1b,cr}^* = {}_{CP}^{(2)}U_{2b,cr}^*$

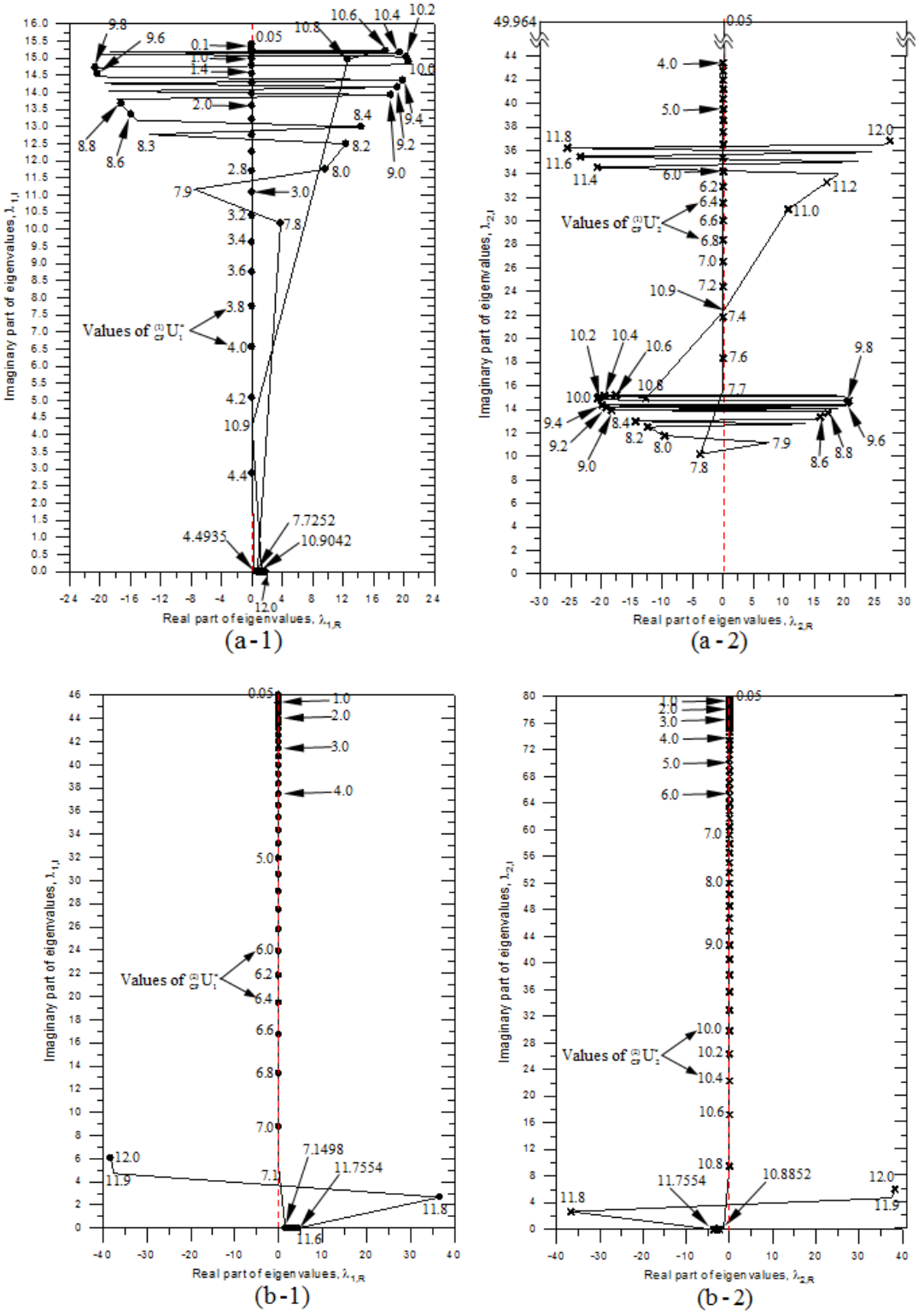

Figure 10: The Argand Diagrams for the 1st and 2nd Complex Eigen Values of (a) 1-, (b) 2-, (c) 3- and (d) 4- Span Fluid-Conveying C-P Pipes Shown in Figs.9(a)-(d) with Mass Ratio $m_f^* = 0.5$. In Other Words, (a-1) and (a-2) are Those of *1-span* pipe; (b-1) and (b-2) are those of *2-span* pipe; (c-1) and (c-2) are those of *3-Span* Pipe; and (d-1) and (d-2) are those of *4-Span* Pipe

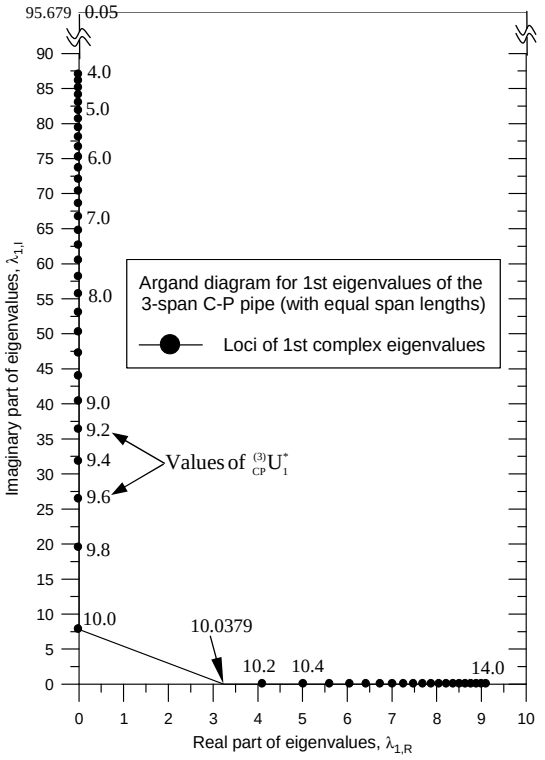

(c-1)

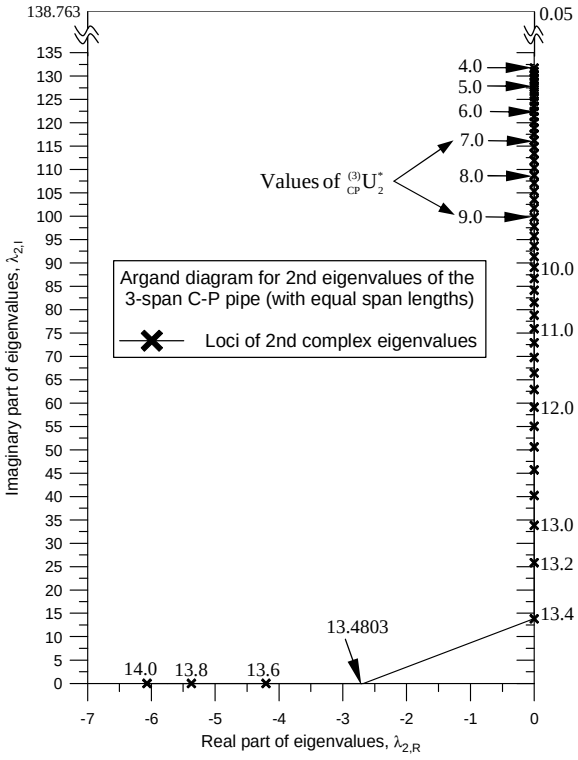

(c-2)

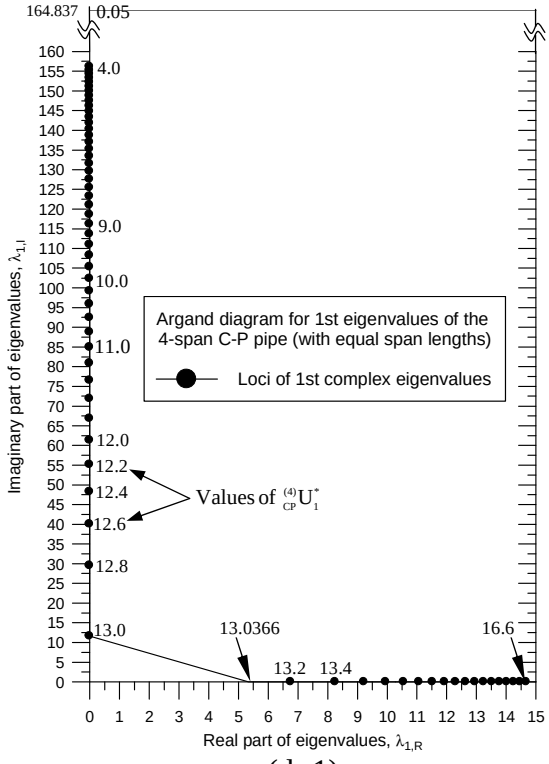

(d-1)

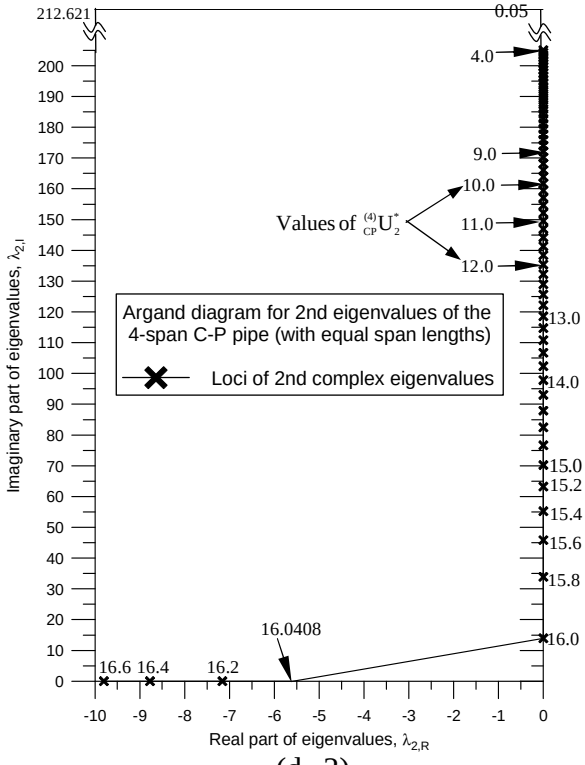

(d-2)

Figure 10: (Continued)

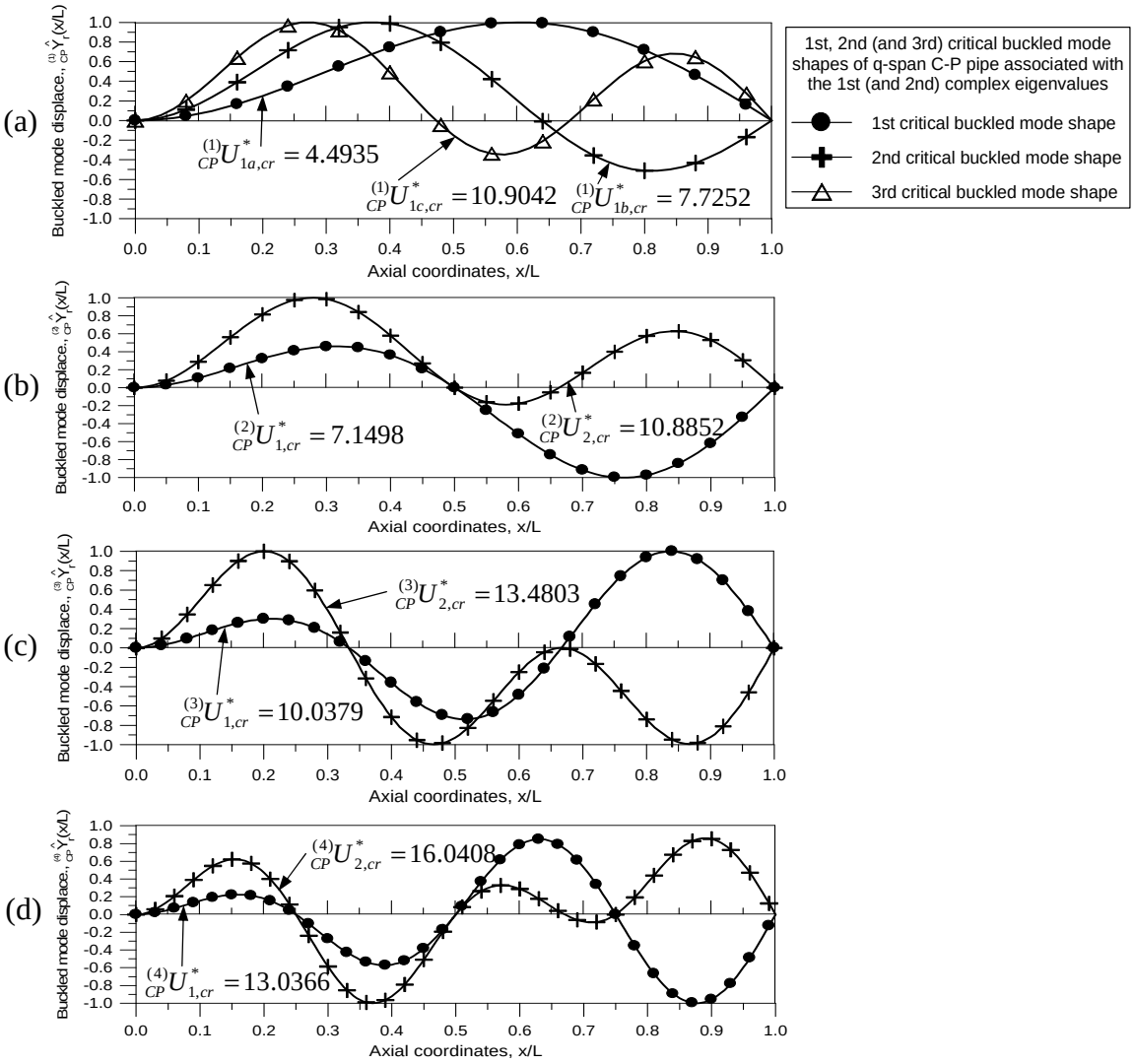

Figure 11: The 1st to 3rd Buckled Mode Shapes of (a) 1-, (b) 2-, (c) 3- and (d) 4- Span Fluid-Conveying C-P Pipes Shown in Figures. 9(a)-(d) with Mass Ratio $m^*_f = 0.5$

3.3 COMPARISON BETWEEN 1st CRITICAL FLOW VELOCITIES FOR P-P, C-C AND C-P PIPES

For comparisons, the 1st critical flow velocities for the 1-, 2-, 3- and 4- span fluid-conveying pipes with P-P, C-C and C-P end conditions are listed in Table 5. In which, the 1st critical flow velocities shown in the 3rd row for the P-P pipe, $^{(q)}_{PP}U^*_{1,cr}$ (with $q = 1,2,3,4$), are obtained from the Argand diagrams shown in Figure 4(a-1), (b-1), (c-1) and (d-1), respectively; those shown in the 4th row for the C-C pipe, $^{(q)}_{CC}U^*_{1,cr}$ (with $q = 1,2,3,4$), are obtained from Figure 7(a-1), (b-1), (c-1) and (d-1), respectively; and those shown in the 5th row for the C-P pipe, $^{(q)}_{CP}U^*_{1,cr}$ (with $q = 1,2,3,4$), are obtained from Figure 10(a-1), (b-1), (c-1) and (d-1), respectively. From Table 5 one sees that:

- For a "*q*-span" P-P pipe with equal span lengths, its 1st critical flow velocity of buckling is given by $^{(q)}_{PP}U^*_{1,cr} = q\pi$, which is equal to the *r*th *equivalent* critical flow velocity obtained from the theory of *static* stability (for the classical axial-loaded "1-span" P-P *beam*), $_{PP}V^*_{r,cr} = r\pi$, i.e., $^{(q)}_{PP}U^*_{1,cr} = {}_{PP}V^*_{r,cr} = r\pi$ (with $q = r$). Since the

expression ${}_{PP}V^*_{r,cr}=r\pi$ obtained from the theory of *static* stability is independent on the mass ratio m^*_f, so is the expression ${}^{(q)}_{PP}U^*_{1,cr}={}_{PP}V^*_{r,cr}=r\pi$ (with $q=r$). The last relationship is not available for the "*q*-span" ($q\geq 1$) pipe with the other end conditions (such as C-C or C-P).

- For an "1-span" pipe with *S* end conditions (with *S* = P-P, C-C or C-P), its 1st critical flow velocity obtained from the theory of *dynamic* stability presented in this paper, ${}^{(1)}_{S}U^*_{1,cr}$, is equal to the 1st *equivalent* one obtained from the theory of *static* stability shown in the *Appendix* (of this paper), ${}_{S}V^*_{1,cr}$, i.e., ${}^{(1)}_{S}U^*_{1,cr}={}_{S}V^*_{1,cr}$.

- Among the 1st critical flow velocities of the "1-span" P-P, C-C and C-P pipes, the order of the magnitudes is ${}^{(1)}_{PP}U^*_{1,cr}<{}^{(1)}_{CP}U^*_{1,cr}<{}^{(1)}_{CC}U^*_{1,cr}$, this is reasonable because the stiffness of the P-P pipe is smallest and that of the C-C pipe is largest. The last trend is also true for the "*q*-span" pipes, i.e. ${}^{(q)}_{PP}U^*_{1,cr}<{}^{(q)}_{CP}U^*_{1,cr}<{}^{(q)}_{CC}U^*_{1,cr}$ with $q\geq 2$, and the divergences between them decrease with the increase of span number *q*.

Table 5: The "first" Critical Dimensionless flow Velocities ${}^{(q)}_{S}U^*_{1,cr}$ of the "*q*-span" Fluid-Conveying *Pipe* with *S* BCs and the Lowest "four" *Equivalent* Critical ones ${}_{S}V^*_{r,cr}$ ($r=1\sim 4$) of the Classical Axial-Loaded "1-span" *beam* with *S* BCs

BCs for *q*-Span *Pipe S*	"First " Critical Dimensionless Flow Velocities of "*q*-Span" *Pipe*, ${}^{(q)}_{S}U^*_{1,cr}$			
	${}^{(1)}_{S}U^*_{1,cr}$ ([a] $q=1$)	${}^{(2)}_{S}U^*_{1,cr}$ ($q=2$)	${}^{(3)}_{S}U^*_{1,cr}$ ($q=3$)	${}^{(4)}_{S}U^*_{1,cr}$ ($q=4$)
P-P	π	2π	3π	4π
C-C	2π	8.9869	11.5701	14.2995
C-P	4.4935	7.1498	10.0379	13.0366
BCs for axial-loaded 1-span ($q=1$) *beam S*	Lowest "four" *equivalent* critical dimensionless flow velocities of "1-span" *beam*, ${}_{S}V^*_{r,cr}$			
	${}_{S}V^*_{1,cr}$ ([b] $r=1$)	${}_{S}V^*_{2,cr}$ ($r=2$)	${}_{S}V^*_{3,cr}$ ($r=3$)	${}_{S}V^*_{4,cr}$ ($r=4$)
P-P	π (=3.1416)	2π (=6.2832)	3π (=9.4248)	4π (=12.5664)
C-C	2π (=6.2832)	4π (=12.5664)	6π (=18.8496)	8π (=25.1328)
C-P	4.4935	7.7253	10.9041	14.0662

[a] *q* = total number of *spans* for each *pipe*

[b] *r* = *mode* number for a specified vibration of *beam*

3.4 FREE VIBRATION ANALYSES OF A 4-SPAN PIPE WITH VARIOUS END CONDITIONS

In general, the 1st critical flow velocities obtained in the last subsection are much higher than the realistic ones, thus, this subsection illustrates a practical example to show the influence of fluid pressure intensity p_f, flow velocity *U* and Coriolis force on the lowest four natural frequencies ω_r of a 4-span fluid-conveying pipe with P-P, C-C and C-P end conditions as shown in Figure 2(d), 6(d) and 9(d), respectively. The dimensions and physical properties of the pipes are the same as those mentioned at the beginning of this section: outer diameter $d_o=0.254$ m, inner diameter $d_i=0.2286$ m, Young's modulus $E=2.068\times10^{11}$ N/m^2, mass density of pipe $\rho_p=7850$ kg/m^3, mass density of water (outside the pipe) $\rho_w=1000$ kg/m^3 and total length of the pipe $L=6\times4=24$ m. Besides, we assume that the mass density of fluid (inside the pipe) is $\rho_f=1000$ kg/m^3 and the externally applied axial-load is $P_p=1.0\times10^6$ N. Three cases are studied:

Case 1 is with $p_f = U = 0$ (no fluid pressure and no Coriolis force); Case 2 is with $p_f = 1.0\times10^5$ N/m^2 and $U = 20$ m/s (with Coriolis force neglected); Case 3 is the same as Case 2 except that the Coriolis force is considered. The results are listed in Table 6 with total elements for each pipe to be $n_e = 50\times4 = 200$. Since each node has two DOFs, the total *effective* DOFs for the 4-span P-P, C-C and C-P pipes are 397, 395 and 396, respectively. Among the three pipes, the total *effective* DOFs of the P-P pipe is largest so that its stiffness is smallest, on the contrary, the total *effective* DOFs of the C-C pipe is smallest so that its stiffness is largest. This is the reason why the order for the lowest four natural frequencies of the three pipes is: ${}^{(4)}_{PP}\omega_r < {}^{(4)}_{CP}\omega_r < {}^{(4)}_{CC}\omega_r$ (with $r = 1-4$) as one may see from Table 6 for either Case 1, Case 2 or Case 3. From Table 6 one also sees that either the "effective axial load" due to fluid pressure $p_f A_f$ as well as centrifugal force $m_f U^2$ or the "Coriolis force" can reduce the lowest four natural frequencies of the fluid-conveying pipe, however, the effect of the "Coriolis force" is much smaller than that of the "effective axial load".

Table 6: Influence of Fluid Pressure Intensity p_f, Flow Velocity *U* and Coriolis Force on the Lowest Four Natural Frequencies ω_r of a 4-Span Fluid-Conveying Pipe with P-P, C-C and C-P End Conditions Shown in Figure 2(d), 6(d) and 9(d). ($\rho_f = 1000$ kg/m^3 and $P_p = 1.0\times10^6$ N)

Case	Pressure Intensity p_f (N/m^2)	Flow Velocity U (m/s)	Is Coriolis force considered?	End conditions *S*	Natural Frequencies ω_r (Rad/Sec)			
					ω_1	ω_2	ω_3	ω_4
1 (Undamped)	0	0	No	P-P	69.9263	84.6625	118.3916	156.5799
				C-C	84.6625	118.3916	156.5799	177.4897
				C-P	73.8766	100.1403	137.8284	171.4725
2 (Undamped)	1.0×10^5	20	No	P-P	69.6854	84.4540	118.2250	156.4430
				C-C	84.4540	118.2250	156.4430	177.3712
				C-P	73.6458	99.9546	137.6775	171.3480
3 (Damped)	1.0×10^5	20	Yes	P-P	69.6782	84.4457	118.2152	156.4319
				C-C	84.4457	118.2152	156.4318	177.3588
				C-P	73.6383	99.9455	137.6670	171.3361

Figure 12(a)-(c) show the lowest four *natural* mode shapes of the 4-span pipe, ${}^{(4)}_{S}Y_r(x)$ ($r = 1-4$). In which, Figure 12(a) is for the P-P pipe, ${}^{(4)}_{PP}Y_r(x)$, Figure 12(b) is for the C-C pipe, ${}^{(4)}_{CC}Y_r(x)$, and Figure 12(c) is for the C-P pipe, ${}^{(4)}_{CP}Y_r(x)$. It is noted that the solid curves (——) with symbols, O, ×, △ and □, denote the 1st, 2nd, 3rd and 4th *un-damped* mode shapes (for Case 1), respectively, while the dashed curves (– – –) with symbols, ●, ✚, ▲ and ■, denote the corresponding *damped* ones (for Case 3), respectively. Since the *un-damped* natural frequencies are very close to the corresponding *damped* ones as shown in Table 6, so are the associated natural mode shapes as one may see from Figure 12.

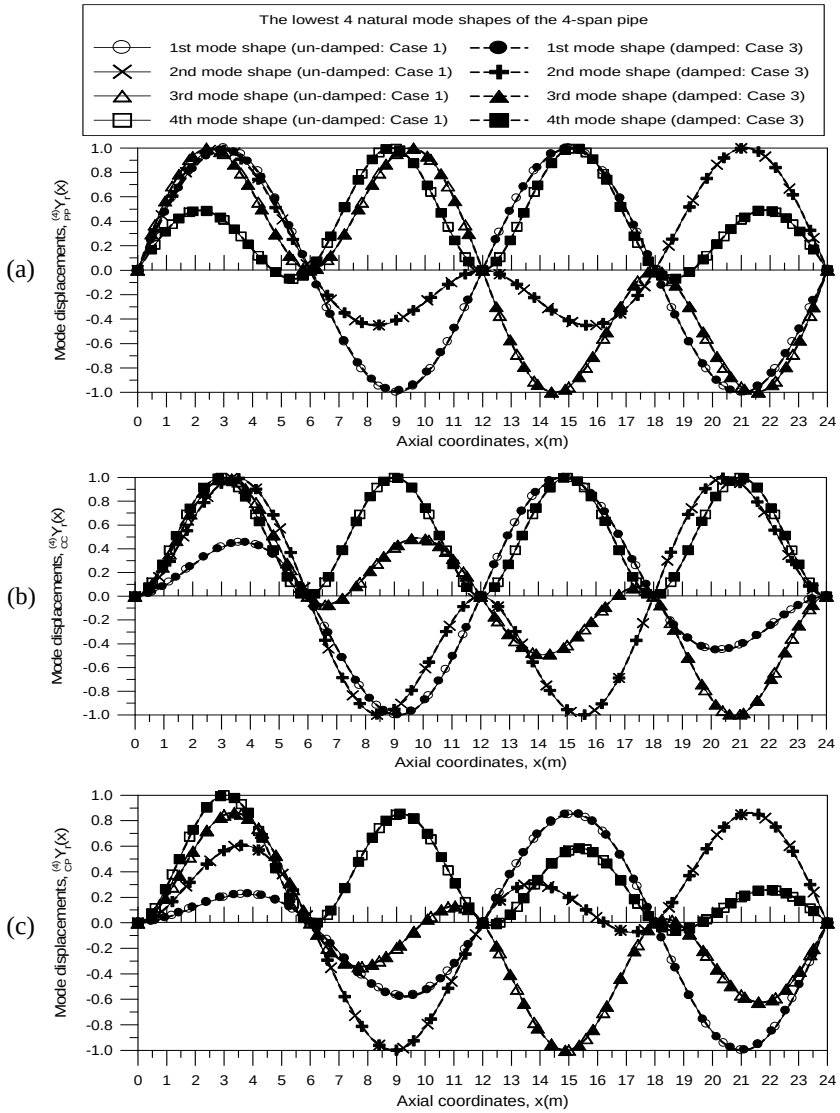

Figure 12: The Lowest Four *Natural* Mode Shapes of a 4-Span Pipe with Three End Conditions: (a) P-P, (b) C-C and (c) C-P. Where The solid Curves, —O—, —×—, —△—and —□—, denote the 1st, 2nd, 3rd and 4th *un-Damped* Mode Shapes (Case 1), while the Dashed Curves, ---●---, ---✚---, ---▲--- and ---■---, Denote the Corresponding *Damped* Ones (Case 3).

4. CONCLUSIONS

Based on the foregoing numerical results and discussions, we draw the following conclusions:

- For an "1-span" fluid-conveying pipe with *S* end conditions (with *S* = P-P, C-C or C-P), its "1st" critical flow velocity obtained from the theory of *dynamic* stability presented in this paper, $^{(1)}_{S}U^{*}_{1,cr}$, is equal to the "1st" *equivalent* one obtained from the theory of *static* stability (for the classical axial-loaded "1-span" *beam*) shown in the *Appendix*, $_{S}V^{*}_{1,cr}$, i.e., $^{(1)}_{S}U^{*}_{1,cr}=_{S}V^{*}_{1,cr}$. This is a reasonable result, because, according to the theory of either *dynamic* or *static* stability, the first critical flow velocity is obtained from the condition that the first natural frequency of the vibrating system approaches zero (i.e. $\omega_1 \approx 0$). This reasonable result may also be one of the evidences that the theories presented in the text and the appendix of this paper should be reliable.

- Since the "1st" critical buckled *mode shapes* of the one-, two-, three- and four- *span* fluid-conveying "P-P *pipes*" with identical span lengths, ${}^{(q)}_{PP}\hat{Y}_{1,cr}(\xi)$ ($q=1-4$), take the same forms as the 1st, 2nd, 3rd and 4th buckled *mode shapes* of the classical axial-loaded "1-span" P-P *beam*, ${}_{PP}\hat{Z}_{r,cr}(\xi)$ ($r=1-4$), respectively, and the *equivalent* "*r*th" dimensionless critical flow velocity of buckling for the latter *beam* is given by ${}_{PP}V^*_{r,cr}=r\pi$, the corresponding "1st" dimensionless critical flow velocity of buckling for the "*q*-span" P-P *pipe* (with identical span lengths) is given by ${}^{(q)}_{PP}U^*_{1,cr}={}_{PP}V^*_{r,cr}=q\pi$ (with $q=r$). The last relationship ${}^{(q)}_{PP}U^*_{1,cr}=q\pi$ is not available for the "*multi*-span" C-C or C-P *pipe*.
- For the "1-span" fluid-conveying *pipe* with P-P, C-C and C-P BCs, the stiffness of the P-P pipe is smallest and that of the C-C pipe is largest, so that the magnitude order for the associated "1st" critical flow velocities is: ${}^{(1)}_{PP}U^*_{1,cr}<{}^{(1)}_{CP}U^*_{1,cr}<{}^{(1)}_{CC}U^*_{1,cr}$. This conclusion is also true for the "*q*-span" fluid-conveying pipe, i.e. ${}^{(q)}_{PP}U^*_{1,cr}<{}^{(q)}_{CP}U^*_{1,cr}<{}^{(q)}_{CC}U^*_{1,cr}$ with $q\geq 2$, and the divergences between them decrease with the increase of the total span number *q*.
- For the "1-span" P-P, C-C or C-P fluid-conveying pipe, all three critical dimensionless flow velocities (${}^{(1)}_{S}U^*_{1a,cr}$, ${}^{(1)}_{S}U^*_{1b,cr}$ and ${}^{(1)}_{S}U^*_{1c,cr}$) are associated with the "1st" complex eigenvalues (λ_1). It is found that the pipe will be buckled (and lose stiffness) if the flow velocity ${}^{(1)}_{S}U^*_1$ is greater than the "1st" or "3rd critical one (i.e., ${}^{(1)}_{S}U^*_1>{}^{(1)}_{S}U^*_{1a,cr}$ or ${}^{(1)}_{S}U^*_1>{}^{(1)}_{S}U^*_{1c,cr}$) and will restore stability (or regain stiffness) if the flow velocity is greater than the 2nd critical one (i.e., ${}^{(1)}_{S}U^*_1>{}^{(1)}_{S}U^*_{1b,cr}$). Since the pipe regains its stiffness when ${}^{(1)}_{S}U^*_1>{}^{(1)}_{S}U^*_{1b,cr}$ and will be buckled again when ${}^{(1)}_{S}U^*_1>{}^{(1)}_{S}U^*_{1c,cr}$, this may be the reason why the *imaginary* part of the "1st" complex eigenvalue ($\lambda_{1,I}$) is equal to that of the "2nd" one ($\lambda_{2,I}$), i.e., $\lambda_{1,I}=\lambda_{2,I}$, and the *real* part of the "1st" complex eigenvalue ($\lambda_{1,R}$) is "opposite" to that of the "2nd" one ($\lambda_{2,R}$), i.e., $\lambda_{1,R}=-\lambda_{2,R}$, if the flow velocity ${}^{(1)}_{S}U^*_1$ is greater than the 2nd and less than the 3rd critical ones by about 0.2, i.e., $({}^{(1)}_{S}U^*_{1b,cr}+0.2)<{}^{(1)}_{S}U^*_1<({}^{(1)}_{S}U^*_{1c,cr}-0.2)$. In other words, for the last case, the oscillations of the pipe are first-and-second-mode-coupled.
- Except for the 3-span C-C pipe, for a "*q*-span" P-P, C-C or C-P pipe with $q\geq 2$, the 1st critical flow velocity (${}^{(q)}_{S}U^*_{1,cr}$) is only associated with the 1st complex eigenvalue (λ_1) and the 2nd critical flow velocity (${}^{(q)}_{S}U^*_{2,cr}$) is only associated with the 2nd complex eigenvalue (λ_2), so that the corresponding critical buckled mode shapes, ${}^{(q)}_{S}\hat{Y}_{1,cr}(\xi)$ and ${}^{(q)}_{S}\hat{Y}_{2,cr}(\xi)$, are not coupled.
- The main difference between the critical flow velocity leading to buckling of the fluid-conveying *pipe* obtained from the theory of *dynamic* stability presented in this paper, ${}^{(q)}_{S}U^*_{r,cr}$, and the "equivalent" one obtained from the theory of *static* stability (for the classical axial-loaded "1-span" *beam*) shown in the ***Appendix***, ${}_{S}V^*_{r,cr}$, is the Coriolis force arising from the flowing fluid, thus, the buckled mode shape associated with the "1st" complex

eigenvalue appearing in the fluid-conveying *pipe* and missing in the classical axial-loaded "1-span" *beam* is due to the Coriolis effect, and so is the first-and-second-mode-coupled vibrations of the fluid-conveying *pipe*. In other words, the information about restoring stability of the *pipe* from its buckling state and coupling oscillations of the 1st and 2nd modes can only be obtained from the theory of *dynamic* stability.

- For the 3-span C-C pipe, although the pipe restores its stiffness at the *second* critical flow velocity (${}^{(3)}_{CC}U^{*}_{1b,cr}$) associated with the "1st" complex eigenvalue (λ_1) and the latter is equal to the *second* critical flow velocity (${}^{(3)}_{CC}U^{*}_{2b,cr}$) associated with the "2nd" complex eigenvalue (λ_2), i.e. ${}^{(3)}_{CC}U^{*}_{1b,cr} = {}^{(3)}_{CC}U^{*}_{2b,cr} = 17.3924$, it is found that, in the last condition, the corresponding buckled mode shape associated with λ_1 is different from that associated with λ_2 as one may see from Figure 8(c). This result is reasonable, because the (buckled) mode shapes are dependent on the corresponding eigenvalues (λ_1 and λ_2) and $\lambda_1 = \lambda_{1,R} + i\lambda_{1,I}$ in not equal to $\lambda_2 = \lambda_{2,R} + i\lambda_{2,I}$ (i.e., $\lambda_1 \neq \lambda_2$) as one may see from column 11 of Table 3(b).

- Besides the stability analysis, the presented FEM is also available for studying the influence of certain parameters on the free vibration characteristics of a *multi-span* fluid-conveying pipe subjected to arbitrary externally applied axial-load P_p, internal fluid pressure intensity p_f and fluid velocity U with various end supports (or BCs). For the 4-span fluid-conveying pipe with P-P, C-C and C-P BCs studied, it has been found that either the "effective axial load" due to fluid pressure as well as centrifugal force or the "Coriolis force" can reduce the lowest four natural frequencies, however, the effect of the "Coriolis force" is much smaller than that of the "effective axial load".

APPENDIX

Equivalent Critical Flow Velocities and Buckled Mode Shapes for a *Single-Span* Fluid-Conveying Pipe Obtained from Theory of *Static* Stability

A.1 Axial-Loaded 1-Span P-P Beam

According to the theory of *static* stability [30], the *r*th critical buckling load of an axial-loaded *1-span* P-P beam (in air) is given by

$${}_{PP}N_{r,cr} = EI(r\pi/L)^2 \tag{A.1}$$

For the case with $P_p = p_f A_f = 0$, from Eq. (16c) one obtains the *equivalent* axial load

$$N = m_f V^2 \tag{A.2}$$

Where the flow velocity U is replaced by the *equivalent* one V, for convenience.

From Eqs. (A.1) and (A.2), one obtains the *r*th equivalent *critical* flow velocity of buckling for a *single-span* P-P pipe to be

$${}_{PP}V_{r,cr} = (r\pi/L)\sqrt{EI/m_f} \tag{A.3}$$

According to Eq. (23b), the corresponding *r*th *dimensionless* critical flow velocity is given by

$$_{PP}V^{*}_{r,cr} = V_{r,cr}L\sqrt{m_f/(EI)} = r\pi \tag{A.4}$$

Furthermore, from Ref. [30], one obtains the following *r*th critical buckled mode shape

$$_{PP}\hat{Z}_{r,cr}(x) = \overline{A}_r \sin\alpha_r x \tag{A.5}$$

Since

$$\alpha_r = \sqrt{_{PP}N_{r,cr}/(EI)} = r\pi/L \tag{A.6}$$

The substitution of Eq. (A.6) into Eq. (A.5) produces

$$_{PP}\hat{Z}_{r,cr}(x) = \overline{A}_r \sin(r\pi x/L) \tag{A.7}$$

For $\overline{A}_r = 1.0$, one has lowest four critical buckled "unit-amplitude" mode shapes as shown in Figure A.1(a).

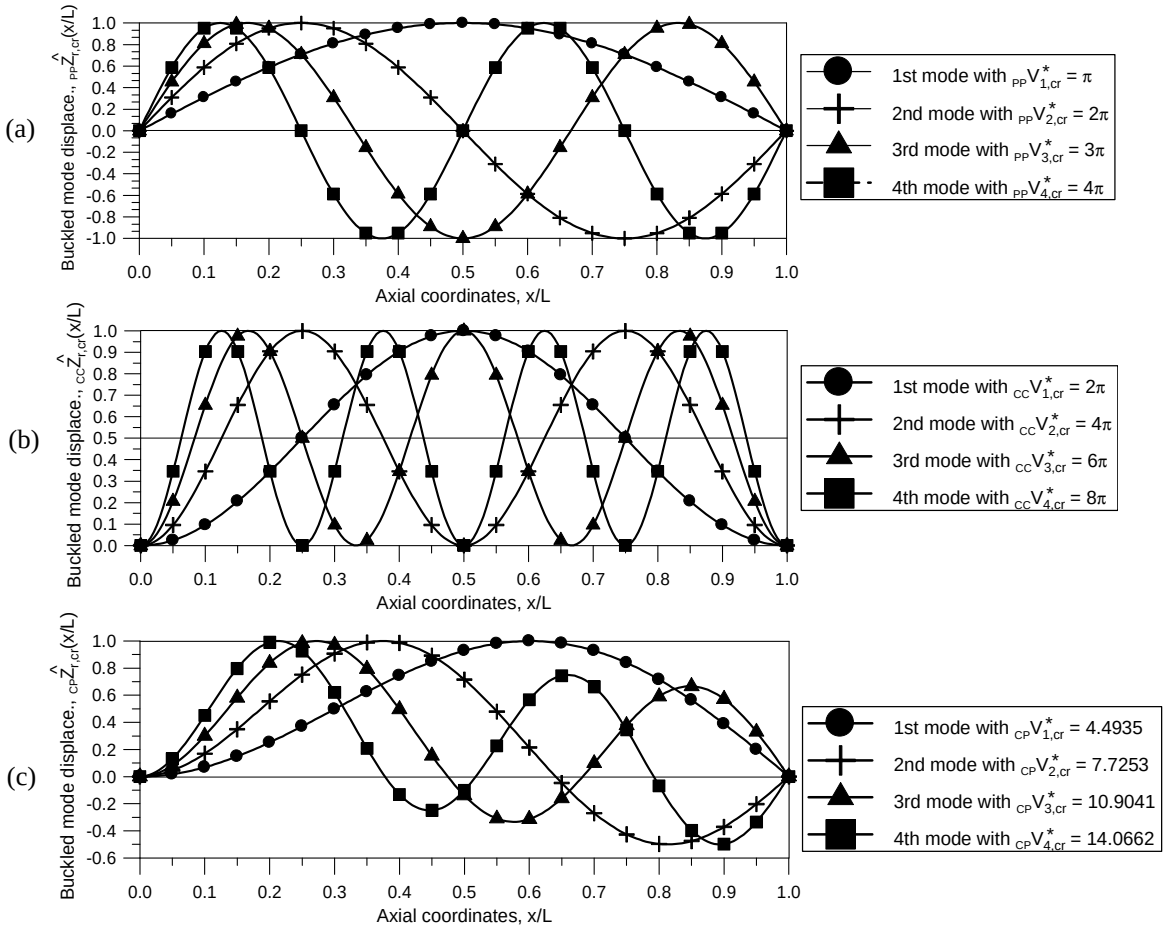

Figure A.1: The Lowest 4 Critical Buckled "Unit-Amplitude" Mode Shapes of a Uniform Axial-Loaded 1-Span (a) P-P, (b) C-C and (c) C-P Beams with the Curves Attached by SYMBOLS, ●, +, ▲ and ■, Denoting the 1st, 2nd, 3rd and 4th Ones, Respectively

A.2 Axial-Loaded 1-Span C-C Beam

The *r*th critical buckling load of an axial-loaded *1-span* C-C beam is given by [30]

$$_{CC}N_{r,cr} = 4EI\,(r\pi/L)^2 \tag{A.8}$$

For the case with $P_p = p_f A_f = 0$, from Eq. (16c) one obtains $N = m_f V^2$, thus, the *equivalent* *r*th critical flow velocity of buckling is given by

$$_{CC}V_{r,cr} = 2(r\pi/L)\sqrt{EI/m_f} \tag{A.9}$$

Thus, from Eq. (23b), the corresponding *r*th dimensionless critical flow velocity is

$$_{CC}V^*_{r,cr} = {}_{CC}V_{r,cr}L\sqrt{m_f/(EI)} = 2r\pi \tag{A.10}$$

Furthermore, from [30], one obtains the *r*th critical buckled mode shape to be

$$_{CC}\hat{Z}_{r,cr}(x) = \overline{A}_r(1-\cos\alpha_r x) \tag{A.11}$$

Since

$$\alpha_r = \sqrt{{}_{PP}N_{r,cr}/(EI)} = 2r\pi/L \tag{A.12}$$

The substitution of Eq. (A.12) into Eq. (A.11) leads to

$$_{CC}\hat{Z}_{r,cr}(x) = \overline{A}_r[1-\cos(2r\pi x/L)] \tag{A.13}$$

For $\overline{A}_r = 0.5$, one has lowest four critical buckled "unit-amplitude" mode shapes as shown in Figure A.1(b).

A.3 Axial-loaded 1-span C-P beam

The *r*th critical buckling load of an axial-loaded *1-span* C-P beam is given by [33]

$$_{CP}N_{r,cr} = \varepsilon_r^2 EI \tag{A.14}$$

For the case with $P_p = p_f A_f = 0$, from Eq. (16c) one obtains $N = m_f V^2$, thus, the *equivalent* *r*th critical flow velocity of buckling is given by

$$_{CP}V_{r,cr} = \varepsilon_r\sqrt{EI/m_f} \tag{A.15}$$

Now, from the above equation and Eq. (23b), one obtains the corresponding *r*th dimensionless critical flow velocity

$$_{CP}V^*_{r,cr} = {}_{CP}V_{r,cr}L\sqrt{m_f/(EI)} = \varepsilon_r L \tag{A.16}$$

Furthermore, from Ref. [33], one obtains the following *r*th critical buckled mode shape

$$_{CP}\hat{Z}_{r,cr}(x) = \overline{A}_r[\sin\varepsilon_r L\xi - \varepsilon_r L\cos\varepsilon_r L\xi + \varepsilon_r L(1-\xi)] \tag{A.17}$$

Where $\xi = x/L$.

Since Figure 2.17 of Ref. [33] reveals that

$$\varepsilon_r L = 4.4935, 7.7253, 10.9041, 14.0662 \text{ (for } r = 1\text{- } 4) \quad \text{(A.18)}$$

from Eqs. (A.17) and (A.18) one obtains the lowest four unit-amplitude critical buckled mode shapes of the C-P beam as shown in Figure A.1(c).

REFERENCES

1. *Ibrahim, R.A. (2010). Overview of mechanics of pipes conveying fluids-Part I: fundamental studies. Journal of Pressure Vessel Technology, Transactions of the ASME. 132, 034001-32.*
2. *Chen, S.S. (1971). Dynamic stability of a tube conveying fluid, Journal of the Engineering Mechanics Division, Proceedings of the ASCE. 97, 1469-1485.*
3. *Paidoussis, M.P., Issid, N.T. (1974). Dynamic stability of pipes conveying fluid. Journal of Sound and Vibration. 33, 267-294.*
4. *Ting, E. C., Hosseinipour, A. (1986). A numerical approach for flow-induced vibration of pipe structures, Journal of Sound and Vibration. 88, 289-298.*
5. *Paidoussis M.P., Luu, T.P., Laithier B.E. (1986). Dynamics of finite-length tubular beams conveying fluid. Journal of Sound and Vibration. 106, 311-331.*
6. *Chen, W.H., Fan, C.N. (1987). Stability analysis with lumped mass and friction effects in elastically supported pipes conveying fluid. Journal of Sound and Vibration. 119, 429-442.*
7. *Pramila, A., Laukkanen, J., Liukkonen, S. (1991). Dynamics and stability of short fluid-conveying Timoshenko element pipes. Journal of Sound and Vibration. 144, 421-425.*
8. *Dupuis, C., Rousselet, J. (1992). Discussion on 'Dynamics and stability of short fluid-conveying Timoshenko element pipes'. Journal of Sound and Vibration. 152, 561-563.*
9. *To, C.W., Healy, J.W. (1986). Further comment on 'Vibration analysis of straight and curved tubes conveying fluid by means of straight beam finite elements'. Journal of Sound and Vibration. 105, 513-514.*
10. *Pramila, A. (1986). On the gyroscopic terms appearing when the vibration of fluid-conveying pipes is analyzed using the FEM. Journal of Sound and Vibration. 105, 515-516.*
11. *Chang, C.O., Cheng, K.C. (1994). Dynamics and stability of pipes conveying fluid. Journal of Pressure Vessel Technology. 116, 57-66.*
12. *Bratt, J. (1995). Lateral vibration of fluid-conveying pipes. Structure Engineering Review. 7, 15-21.*
13. *Stein, R.A., Tobriner, M.W. (1970). Vibration of pipes containing flowing fluids. Journal of Applied Mechanics, Transactions of the ASME. 37, 906-916.*
14. *Singh, K., Mallik, A.K. (1977). Wave propagation and vibration response of a periodically supported pipe conveying fluid. Journal of Sound and Vibration. 54, 55-66.*
15. *Singh, K., Mallik, A.K. (1979). Parametric instabilities of a periodically supported pipe conveying fluid. Journal of Sound and Vibration. 62, 379-397.*
16. *Koo, G..H., Park, Y.S. (1998). Vibration reduction by using periodic supports in piping system. Journal of Sound and Vibration. 210, 53-68.*
17. *Wu, J.S., Shih, P.Y. (2001). The dynamic analysis of a multi-span fluid-conveying pipe subjected to external load. Journal of Sound and Vibration. 239, 201-215.*

18. *Wu, J.S., Lo, S.C., Chao, R.M. (2015). Dynamic stability and free vibrations of multi-span fluid-conveying pipes. Int. J. of Materials Engineering and Technology, 14(1), 1-43.*
19. *Pilkey, W.D., Chang, P.Y. (1978). Modern Formulas for Statics and Dynamics. McGraw-Hill, New York.*
20. *Clough, R.W., Penzien, J. (1976). Dynamics of Structures. McGraw-Hill, New York.*
21. *Bathe, K.J. (1982). Finite Element Procedures in Engineering Analysis. Prentice-Hall, New York.*
22. *Meirovitch, L. (1967). Analytical Methods in Vibrations, Macmillan, London.*
23. *Przemieniecki, J.S. (1968). Theory of Matrix Structural Analysis. McGraw-Hill, New York.*
24. *Kohli, A.K., Nakra, B.C. (1984). Vibration analysis of straight and curved tubes conveying fluid by means of straight beam finite elements. Journal of Sound and Vibration. 93(2), 307-311.*
25. *Pramila, A. (1992). Author's reply: Any extended form of Hamilton's principle can be applied to non-conservative straight fluid-pipe systems, Journal of Sound and Vibration. 152(3), 564-566.*
26. *Aldraihem, O.J. (2007). Analysis of the dynamic stability of collar-stiffened pipes conveying fluid. Journal of Sound and Vibration. 300, 453-465.*
27. *Wu, J.S., Chen, K.W. (2003). An alternative approach to the structural motion analysis of wedge-beam offshore structures supporting a load. Ocean Engineering. 30(14), 1791-1806.*
28. *Wu, J.S., Chen, C.T. (2007). Forced vibration analysis of an offshore tower carrying an eccentric tip mass with rotary inertia due to support excitation. Ocean Engineering. 34, 1235-1244.*
29. *Garbow, B.S. (1977). Matrix Eigensystem Routines-EISPACK Guide Extension. Springer-Verlag, Berlin.*
30. *Timoshenko, S.P., Gere, J.M. (1977). Mechanics of Materials, McGraw-Hill, New York.*
31. *Busool, W., Eisenberger, M. (2002). Vibrations of axially loaded continuous beams. Int. J. of Structural Stability and Dynamics. 2, 117-133.*
32. *Gregory, R.W., Paidoussis, M.P. (1966). Unstable oscillation of tubular cantilevers conveying fluid. I. Theory. Proceedings of Royal Society (London). 293(A), 512-527.*
33. *Wu, J.S. (2013). Analytical and Numerical Methods for Vibration Analyses. John Wiley & Sons, Singapore Pte. Ltd.*